This manuscript is a revised preprint and has been re-submitted for publication in **Basin Research**. The current version covers two rounds of peer review but is **not yet accepted for publication**. Subsequent versions of this manuscript may differ due to additional peer review or the editorial process. If accepted for publication, the final version will be available through the "Peer-reviewed publication DOI" link on EarthArxiv.
We hope you find this paper interesting and would welcome your feedback on it. Kindly contact Folarin Kolawole (*folarin.kol@gmail.com*) with your feedback.

Rift Interaction Zones and the Stages of Rift Linkage in Active Segmented Continental Rift Systems

Folarin Kolawole[1,2*], Max C. Firkins[1], Thuwaiba S. Al Wahaibi[1], Estella A. Atekwana[3], Michael J. Soreghan[1]

[1]School of Geosciences, University of Oklahoma, 100 East Boyd Street, RM 710, Norman, OK 73019
[2]Now at BP America, 501 Westlake Park Blvd, Houston, TX 77079
[3]Department of Earth Sciences, University of Delaware, 101 Penny Hall, Newark, DE 19718

**Corresponding Author: Folarin Kolawole (folarin.kol@gmail.com)*

Abstract

Although much is known about the interaction of faulting and sedimentation within the basins of active segmented continental rift systems, little is known about these processes within the interaction zones of varying geometries that separate the young interacting segments. We address this problem in the humid, magma-poor juvenile western branch of the East African Rift System (WB-EARS). First, we present a broader classification of rift interaction zone (RIZ) geometries that accommodate both the plan-view geometries and border fault polarity patterns of the interacting rift segments. Within the framework of the RIZ geometries, we explore the large-scale cross-over relief profiles, and the relationships with the spatiotemporal development of rift-linking faults (breaching faults) and axial stream patterns. Our results show that: 1.) distinct long-wavelength 2-D cross-over topographic relief shapes, directionality of axial stream flow (sediment routing patterns), and breaching fault patterns characterize RIZs at the various stages of the linkage of interacting rift basins; 2.) these stages include unbreached, partially-breached, recently-breached, and breached RIZs; 3.) deforming RIZs exhibit different styles of directionality of breaching, including a unidirectional (distinct propagator and receiver segments), bi-directional propagation (both segments act as propagators and receivers), and nucleation and outward propagation of a narrow intra-RIZ subsidiary rift basin; 4.) RIZ breaching is facilitated by rift-flank deformation, and/or rift tip propagation structures in the form of rift splaying, border fault rotation (rift-tip rotation), and fault cluster networks; 5.) the lateral propagation of breaching faults at the rift tips and flanks, facilitated by localized stress concentrations, is modulated by the extension direction and inherited basement structures. Our findings offer a broader insight into the geometries and structural evolution of rift interaction zones, and provide first-order predictions of large-scale sedimentation patterns of humid early-stage continental rift environments. Our models provide testable hypotheses for linking rift architecture and patterns of early-stage sedimentation applicable to ancient rift basins.

Keywords: Continental rifting; Rift interaction; Rift linkage; Normal faults; *Sedimentation*

1. Introduction

Continental extension proceeds, first by the nucleation of discrete, isolated rift basin segments which subsequently propagate laterally towards one another and link-up to form continuous chains of rift basins (Figure 1, e.g., Nelson, et al., 1992; Corti, 2012; Allken et al., 2011, 2012; Zwaan et al., 2016; Molnar et al., 2019; Zwaan and Schreurs, 2020). The cross-over zone of mechanical interaction between the propagating rift segments and rift structures leading to rift segment linkage has been referred to by different terms, which include rift interaction zone (Nelson, et al., 1992; Zwaan et al., 2016), rift accommodation zone (Rosendahl, 1987; Faulds and Varga; 1998; Lambiase and Bosworth, 1995), transfer zone (Morley et al., 1990; Gawthorpe and Leeder, 2000; Corti, 2004; Aanyu and Koehn, 2011; Heilman et al., 2019), and graben stepover zone (Fossen et al., 2010). Here, we adopt the term "Rift Interaction Zone (RIZ)" to describe the large-scale region of rift segment interaction separating individual rift segments within a rift system (following the convention of Nelson, et al., 1992). Rift interaction zones typically host smaller-scale zones of fault interaction and strain transfer which are referred to as "transfer zones" or "accommodation zones" (Rosendahl, 1987; Morley et al., 1990, 1999; Faulds and Varga; 1998; Zwaan and Schreurs, 2020). In this study, we focus on the larger-scale zone of rift segment interactions (RIZs).

The initial localization and structure of rift interaction zones are determined by a variety of factors which include the inherited crustal mechanical anisotropies, variation in strain rate, extension direction, magmatic focusing, border fault and rift geometries etc. (e.g., Bosworth, 1985; Morey et al., 1990; Acocella et al., 1999; Aanyu and Koehn, 2011; Corti, 2012; Heron et al., 2019; Corti et al., 2019). However, rift segment interaction across deforming RIZs occurs in both the early (stretching) and later (necking and hyper-extension) stages of continental rift development (e.g., Aanyu and Koehn, 2011; Pagli et al., 2018; Heilman et al., 2019; La Rosa et al., 2019; Corti et al., 2019; Collanega et al., 2020). At continental break-up, major paleo-RIZs separating the offset segments of a rifted margin may influence the location of subsequent oceanic transform fault development (e.g., Cochran and Martinez, 1988; Behn and Lin, 2000).

Rift interaction zones of active segmented continental rifts are areas of relatively elevated basement which serve as viable source areas for sediment production and supply into the active rift basins which constitute domains of crustal subsidence (Lambiase and Bosworth, 1995). In addition, rift interaction zones may accommodate intense tectonic stresses, seismicity, and magmatism associated with tectonic interactions between active rift segments that are in spatial proximity (Heilman et al., 2019; Corti et al., 2019).

Although climate and sea/lake level change play important roles in sedimentation along continental rifts, the tectonic deformations impose first-order controls on sedimentation patterns and stratigraphic architecture (e.g., Tiercelin et al., 1992; Lambiase and Bosworth, 1995; Soreghan and Cohen, 1996; Soreghan et al., 1999; Hans Nelson et al., 1999; Gawthorpe and Leeder, 2000; Jackson et al., 2005; Mack et al., 2006). Within a given climatic condition, active tectonics impose significant controls on the localization of uplifted zones where erosion and sediment production occur, as well as on the localization of subsidence which serve as depocenters for sediment accumulation (e.g., Hovius, 1998; Gawthorpe and Leeder, 2000; Barnes et al., 2011). Within these settings, the routing of sediments from the uplifted areas into the depocenters are determined by the interplay between tectonic deformation (e.g., spatiotemporal fault interactions), climate, dominant agents of sediment weathering and transport, and base level change (e.g., Allen, 2008).

In evolving continental rift settings, the breaching and burial of cross-over basement-highs between interacting rift basins (RIZs) constitute the dominant signatures of rift linkage and transformation of closed rifts into open rift basins (Gawthorpe and Leeder, 2000). However, there is limited understanding of how the morphology of RIZs evolve with the progression of tectonic and breaching fault interactions between the flanking rift segment pairs. Also, there is a need to better understand how this evolution influences the patterns of sediment routing into the basins, the linkage of the depositional systems, and burial of the pre-existing basement-high of paleo-RIZs.

The first-order characteristic of a rift interaction zone is its geometry (Nelson et al., 1992). Therefore, the systematic assessment of the spatiotemporal evolution of a RIZ requires a consideration of its geometry. However, the existing geometrical classification of RIZs (Nelson et al., 1992) is inadequate, and do not encompass the variety of rift interaction zone geometrical patterns that are observable in several continental rift systems.

In this study, first, we revise the existing classification of RIZ geometries and present a broader classification that provides a better framework for assessing structure and evolutionary stages of RIZs. Within the framework of the broader geometries, we investigate key aspects of the surface morphology and structure of non-magmatic RIZs along the juvenile, humid, magma-poor western branch of the East African Rift System (WB-EARS; Figure 2). Our analyses assess the first order influence of fault breaching and basin-ward denudation on the progressive deformation and burial of the RIZs, and the possible cross-over topographic relief geometries associated with each sequential stage of the RIZ evolution.

1.1. Geologic Setting: The Western Branch of the East African Rift System (WB-EARS)

The western branch of the Cenozoic East African Rift System (WB-EARS; Figure 2) is defined by a N-S-trending arcuate-shaped system of elongate rift basin segments separated by basement rift interaction zones, extending along the Proterozoic mobile belts separating Archean cratons to the east and the west (e.g., Daly et al., 1989; Corti et al., 2007). This rift system branch includes reactivated rift segments that had experienced the earlier phases of Mesozoic extension recorded in east Africa. However, the Cenozoic and Mesozoic rifting events were preceded by the Proterozoic continental accretion of the pre-rift basement. This Precambrian basement of eastern Africa is composed of Proterozoic orogenic belts that wrap around Archean cratonic blocks (Figure 2; Daly et al., 1989; FriRIZ et al., 2013). The rift system propagates along and across the orogenic belts that flank the Tanzanian Craton to the west, which include the Madi-Igisi, Ruwenzori, Ubendian, Kibaran, Irumide, Mozambique, and Zambezi Belts (Figure 2). These mobile belts are dominated by gneisses with granulite and amphibolite facies metamorphic rocks associated with terranes separated by steeply-dipping shear zones and suture zones (Daly et al., 1989).

In the Phanerozoic, eastern Africa experienced at least three phases of continental extension. These phases include the Permo-Jurassic 'Karoo' rifting, Cretaceous rifting, and the currently ongoing Cenozoic phase of rifting (Delvaux, 1989). Some of the currently active segments witnessed the Karoo phase of rifting and were reactivated during the subsequent rifting episodes (e.g., Rukwa, North Malawi, Shire, Luano, and Luangwa Rifts in Figure 2). The Cenozoic rift segments that make up the WB-EARS define a juvenile rift system (<25 Ma; Roberts et al., 2012) extending from the Rhino Rift at its northernmost tip (where the rift system terminates against the NW-trending Precambrian Aswa Shear Zone), southwards through the Malawi Rift, Luangwa, Kundelungu, Mweru, and Kariba Rifts (Figure 2). The southern portions of the western branch (e.g., Luangwa, Kundelungu, Mweru, Mweru-Wantipa, Upemba, and Kariba Rifts) are also referred to as the 'southwestern' segments of the rift system (Daly et al., 2020). In this paper, for simplicity, we consider these 'southwestern' rift segments to be part of the WB-EARS.

The WB-EARS yet remains an enigma, as it is largely magma-poor and its segments have accommodated multiphase crustal stretching since Mesozoic times (Delvaux, 1989; Specht and Rosendahl, 1989; Morley et al., 1999; Simon et al., 2017; Muirhead et al., 2018; Wright et al., 2020). The WB-EARS is currently characterized by a maximum crustal stretching rate of 2.9 mm/yr which is lower in comparison to that of the largely magma-rich eastern branch (up to 5.2 mm/yr) of the East African Rift System, (EB-EARS; Saria et al., 2014). A few magmatic centers occur along the WB-EARS and primarily at the rift interaction zones (Rungwe Volcanic Province (RVP), South Kivu Volcanic Province (SKVP), Toro-Ankole Volcanic Province (TAVP), Virunga Volcanic Province (VVP) in Figure 2). However, most of the interaction zones are generally non-magmatic, showing no evidence of surface volcanism. The absence of surface volcanism in several of the WB-EARS interaction zones present a 'simpler' setting (i.e., one less tectonic variable) to explore the first-order dynamics of early-rift linkage that characterize the growth of continental rifts and break-up process.

2. Data and Methods

Individual rift zones (single or coalesced segments) represent discrete tectonic elements within a rift system, which interact spatially when in proximity to one another. Since active rift basins are zones of active tectonic subsidence, and the intervening cross-over region separating the rifts prior to linkage (rift interaction zone, RIZ; Figure 1) are regions of relatively elevated basement, the linkage of the interacting rifts would require progressive faulting, tectonic subsidence, erosion, and burial of the RIZ cross-over region.

For a satisfactory assessment of the temporal evolution of rift linkage in an active continental rift system as the EARS, we first evaluate the existing classifications of RIZ by examining the East African Rift system and other continental rift systems to create a more robust and useful classification scheme. This updated classification scheme provides a basis for delineating the spatial extent of cross-over region for various RIZ geometries (pink polygons in Figure 3) within which the assessment of breaching structures and cross-over topography can be carried out.

To assess the status of the rift linkage at paired RIZs, we investigate the large-scale patterns of active faulting and cross-over relief profiles across the RIZs. More specifically, we evaluate the similarities and differences in the general patterns of the large-scale cross-over topographic morphology of the non-magmatic RIZs along the WB-EARS (Figure 4a) to identify the prominent trends (e.g., Figures 4b-g). Furthermore, we analyze four representative RIZs that span the possible stages of rift linkage (unbreached, partial breaching, recent breaching, and breached) and contrast the interactions between the tectonic structures and drainage systems in each case. In addition, since the linkage of interacting rifts commonly transforms initially closed rift basins into open basins (Gawthorpe and Leeder, 2000), we extend our assessments to include the first-order trends and geomorphic characteristics of the axial streams that have catchment areas in the RIZs, and/or axial streams that flow across the lengths of the RIZs where observable.

2.1. Cross-Over Topographic Relief Profiles and Axial Stream Morphology

We created topographic profiles of the RIZs from the grids of the Global Multi-Resolution Topography (GMRT) data (Ryan et al., 2009). The terrestrial component of the GMRT data (used in this study) has a spatial resolution of ~30 m. To assess the long-wavelength cross-over topographic geometries of the RIZs, we plot topographic profiles extending between the interacting sift segment pairs, parallel to and orthogonal to the RIZs where appropriate. We present the long-wavelength 2-D cross-over profiles by both the moving average of the 30 m resolution GRMT data, and a profile of resampled GMRT grid (resampled to 4 km resolution). The selection of the localities of the longitudinal topographic profiles are primarily based on the large-scale structure of the examined RIZs. If there exists a zone of fault-bounded valleys linking the interacting rifts (observable on the hillshade topographic and fault maps), we extend the profile through the zone such that each end of the profile is in the axis of one of the two interacting rift basins. If there is no observable linking fault-bounded valley in the RIZ, we place the topographic relief profile at any arbitrary location across the RIZ but ensuring that the two ends of the profile are in the axes of the rift basins.

Due to the unique geometry of overlapping parallel RIZs, we orient the topographic profiles in an across-strike manner (orthogonal to the longitudinal trend of the RIZ).

We emphasize here that in all the WB-EARS RIZs examined in this study, there is no significant large-scale variation in the erodibility of the pre-rift basement lithologies as the areas are primarily dominated by amphibolite-grade gneisses and granulites. In certain areas, the metamorphic basement rocks have been intruded by pre-EARS igneous ring complexes which show more resistance to erosion relative to the gneisses (e.g., Southern Malawi Rift; Nyalugwe et al., 2019a). However, the locations of these igneous intrusions are known, and they are also easily identifiable in the topographic hillshade and aeromagnetic maps. In addition, the intrusions define short-wavelength structures and do not influence the long-wavelength geometries of the important longitudinal topographic relief profiles examined in our study areas. In areas where our profiles intersect the intrusions (e.g., across-rift topographic profiles in Southern Malawi Rift), the intrusions are mostly at the rift margin (border fault domain) and not along the flow path of the axial stream.

To investigate the relationships between the RIZ cross-over topographic relief geometry and the large-scale sediment routing patterns into the interacting rift basins, we plot the longitudinal profiles of rift axial streams (permanent streams) that have catchments in the RIZs using elevation data from the GRMT grid. Although both the axial streams and their tributaries provide sediments from the deforming and eroding RIZ basement-high into the subsiding rift basins, we envision that the large-scale directionality of axial stream flow will more likely be controlled by the slope at the flanks of the RIZs.

The surface textures of the GMRT hillshade digital elevation model (DEM) maps can help delineate the locations of recent alluvial sediment accumulation and areas of crystalline basement exposures (Drury, 2001). Areas characterized by smooth textures on the DEMs are interpreted as depositional surfaces reflecting primarily sediment accumulation and aggradation, with erosion or gullying possibly present, but at a spatial scale lower than the DEM resolution. Areas characterized by rougher textures on the DEM are interpreted as regions of crystalline basement exposures where erosion dominates and produces topographic relief on spatial scales greater than the pixel spacing of the DEM. Thus, to delineate and map areas of subsidence and alluvial sediment accumulation at the propagating tips of the active rift segments, we combine DEM hillshade maps and published surficial geology maps of the study areas (e.g., Choubert et al., 1988). Further, we identify the dominant border fault of a rift segment as the rift-bounding fault that is in the direction of the downward tilt of the basin. Where available, we determine the border fault segments from published seismic reflection images constrained by well log correlation (e.g., Albertine-Rhino RIZ). However, in areas where such subsurface data are absent, we determine the direction of basin tilt from the overall direction of slope of the hanging wall of the basin surface (e.g., Mack et al., 2006).

2.1.1. Stream Sinuosity and Channel Width

In humid continental settings such as the WB-EARS, the linkage of rift basin segments will involve a transformation of at least a part of the RIZ cross-over basement-high (having significant surface slope gradients at the flanks prior to linkage) into a continuous valley floor with significantly lower surface slope gradient after linkage. Since surface slope patterns fundamentally control important geomorphic stream elements such as sinuosity (Lazarus and Constantine, 2013), we assess the patterns of sinuosity along the relevant axial streams.

Our study involves areas of basement exposure and burial along the rift floor near the interacting rift segment tips, therefore, we quantify the variation of the channel width along the axial streams to examine some aspects of the influence of rift-floor basement exposure and RIZ faulting on the large-scale geomorphology of the axial streams within some of the RIZs (e.g., see South Malawi–Shire and Albertine-Rhino RIZs). Since the South Tanganyika-Rukwa RIZ is a parallel RIZ we examine two major streams (Kalambo and "R1" Rivers) that although are not 'axial' to the interacting rifts, are equally relevant to the study as they both initially flow parallel to the RIZ before deflecting into the interacting basins.

We manually digitized the active axial streams analyzed in the representative RIZs, and manually measured the stream widths (perpendicular to the stream channel) at regular intervals along the stream channels using ArcMap© and Google Earth© satellite images. However, due to the difference in the complexity of channel geometry between the study areas (i.e., intensity of channel meandering, presence or absence of braided or anastomosing sections), we varied the intervals used. We obtained measurements at 2 km regular intervals in the Tanganyika - Rukwa RIZs (Kavuu and Luegele Rivers; cumulative stream length of 300 km), 4 km regular intervals in the South Malawi - Shire RIZ (Shire River; total stream length of 200 km), and 1 km regular intervals in the Albertine - Rhino RIZ (Albert Nile River; total stream length of 105 km). At the braided or anastomosing stream segments, we measure the width of the widest active channel. We estimate channel sinuosity of major segments of the axial streams using standard approach. To further assess the axial stream morphology anomalies where relevant, we utilize color composites of Landsat TM optical satellite images obtained from the USGS Earth Explorer database.

2.2. Mapping of Sub-aerial and Subsurface Tectonic Structures

2.2.1. Fault Mapping

To assess the structural deformation in active continental rift interaction zones (i.e., involving at least one active rift segment), there is need for a detailed mapping of both the surface and buried faults, as well as the pre-rift basement fabrics which often influence the patterns of brittle strain localization (e.g., Heilman et al., 2019). In active rift basins, sub-aerial mapping of faults from topographic hillshade maps and in the field are inherently limited because they typically only reveal the recent surface-breaking active fault segments, and are generally not able to delineate the buried active fault segments, which may be accommodating significant tectonic strain (e.g., Kolawole et al., 2018). However, commonly available geophysical datasets such as high-resolution aeromagnetic data provide subsurface imaging of both intra-sedimentary and basement-rooted normal faults (Grauch and Hudson, 2007; Kolawole et al., 2018). Due to the deep-penetrating nature of potential field geophysical signals, aeromagnetic data allows us to discriminate between non-penetrative surface features (such as river and paleo-lake terraces) and mega-scale penetrative structures such as faults and mega-fractures. Unlike the mega-scale penetrative brittle deformation, non-penetrative geological features do not create discontinuity lineaments that offset or disrupt the lateral continuity of basement fabrics at the resolution of the aeromagnetic datasets utilized in this study.

In the representative RIZs analyzed in this study, we utilize the GMRT hillshade DEM and previously published fault maps to delineate the sub-aerial fault segments. For subsurface fault mapping, we evaluate previously published subsurface fault maps and update the maps with subsurface fault interpretations from our filtered high-resolution aeromagnetic maps. For example, in the Tanganyika - Rukwa RIZs, we include and update the previously published surface fault lineaments mapped from satellite topographic hillshade maps and field observations (Delvaux et al., 2012; Muirhead et al., 2018). In the Southern Malawi - Shire RIZ, we include and update previously published surface fault lineaments mapped from satellite topographic hillshade maps and field observations (Wedmore et al., 2020). Also, in the Albertine - Rhino RIZ, we include and update the previously published fault lineaments, some of which were mapped from topographic hillshade maps, seismic reflection datasets, and in the field (GTK Consortium, 2012; Westerhof et al., 2014; Katumwehe et al., 2015; Simon et al., 2017). Therefore, in each of the three representative RIZs analyzed in this study, we identify several subsurface fault segments that are absent in previous publications, and present updated fault maps which enable a detailed structural evaluation of the RIZ deformation.

2.2.2. Mapping of Pre-rift Basement Fabrics

In addition to fault mapping, we utilize the filtered aeromagnetic maps to image and delineate the sub-aerial and buried pre-rift basement fabrics within the representative rift interaction zones in order to better understand the controls on the breach faulting. In the study areas, the pre-rift basement is metamorphic, dominated by gneisses and granulites with mappable foliation trends (Figure 2). In the Tanganyika – Rukwa RIZ, SW Tanzania, we use an aeromagnetic grid of 250 m spatial resolution, collected between 1977-1980 with flight height of 200 m and a flight line spacing of 1 km (Supplementary Figure S1). The Tanzanian aeromagnetic data was provided by the South Africa Development Council (SADC). In the Southern Malawi – Shire RIZ, we utilize a 62 m-resolution aeromagnetic grid, acquired in 2013 at a flight height of 80 m and 250 m flight line spacing (Supplementary Figure S2). The southern Malawi data was provided by the Geological Survey of Malawi (also, freely obtainable from Interdisciplinary Earth Data Alliance, IEDA; Nyalugwe et al., 2019b). In the Albertine - Rhino RIZ, we utilize and update previously published basement fabric interpretations from aeromagnetic data (Supplementary Figure S3; Katumwehe et al., 2015, 2016). Prior to structural interpretation, the Southern Malawi and SW Tanzania aeromagnetic grids were first reduced to the magnetic pole (RTP), and the NW Uganda aeromagnetic data reduced to the magnetic equator (RTE) in order to correctly locate the anomalies over their sources (Arkani-Hamed,1988). After the RTP and RTE corrections, we apply derivative filters to the grids to resolve the structural features following examples of Arkani-Hamed (1988), Ma et al. (2012), and Kolawole et al. (2018).

For our structural analyses, we generate rose diagrams of the frequency-azimuth distribution of the faults and basement fabrics. For multimodal distributions, we divide the data into their modal sets using the frequency minima; and for both the unimodal and multimodal plots, we calculate the circular vector mean and 95 % confidence interval for the modal sets using the method of Mardia and Jupp (2009). All the frequency-azimuth plots are area-weighted.

3. Results

3.1. Re-assessment of Rift Interaction Zone Geometries

Based on our observations of relative geometries of rift segments along the East African Rift System and other continental rift systems, and an evaluation of previously published rift interaction zone classification (Nelson et al., 1992), we present a new classification of RIZ geometries (Figure 3). The terminologies adopted in our new classification are descriptive and refer to the large-scale geometries of the interacting rift segments. Further, where relevant, we include an additional term that accommodates a secondary geometrical or structural component e.g., border fault polarity, and transverse strike/oblique-slip faulting at rift tips.

In this new classification, we distinguish between paired rift transfer zones (involving only 2 rift segments) and compound rift transfer zones (involving more than 2 rift segments). For paired rifts, we account for tip-to-tip, overlapping, and underlapping rift patterns of parallel, oblique, and orthogonal trends of interacting rift pairs (Figure 3). Also, for compound RIZs, we account for triple junction (i.e., involving 3 rift segments) and quadruple junction (i.e., involving 4 rift segments) geometries. Further, we show three possible sub-categories of quadruple junction RIZs in which the adjacent rift segments make oblique or orthogonal angles, or a combination of both with one another. In each class of RIZ geometry, we illustrate the possible lateral extents of the cross-over region. In Oblique Quadruple Junction RIZ, all the adjacent rift segments make oblique angles with one another. In Orthogonal Quadruple Junction RIZ, all the adjacent rift segments make orthogonal angles with one another. Whereas, in the Complex Quadruple Junction, some of the adjacent rift segments make oblique angles with other, whereas the others make orthogonal angles.

Based on our new classification scheme for paired rift segments, we define profile transects across the inter-rift cross-over regions in order to assess the general patterns of the RIZ relief geometries. The following section present our observations of the general patterns of the relief geometries.

3.2. Cross-Over Topographic Relief Profiles of Non-Magmatic Rift Interaction Zones along the Western Branch of the East African Rift System (WB-EARS)

Long-wavelength cross-over topographic relief profiles across the non-magmatic RIZs of different RIZ geometries in the WB-EARS (Figure 4a) exhibit a variety of shapes that can be broadly grouped into four major categories (Type-1 to Type-4) and a sub-category (Type-3-4). We refer to the major categories as Type-1 to Type-4 morphologies (Figures 4b-f). The Type-1 morphology is characterized by high relief; a topographic-high surface, flanked on both sides by generally steep slopes that transition into topographic-low surfaces of the interacting rift segments (e.g., Figure 4b). Examples of the Type-1 morphology include the South Tanganyika–Rukwa (STR-RIZ; 8°S, 31.5°E), Kundelungu–Luapula (KL-RIZ; 10.25°S, 27.75°E), and the Central Luangwa–Central Malawi (CLCM-RIZ; 12°S, 33.5°E) RIZs (see Figure 4a for the locations). The Type-2 morphology is characterized by less pronounced relief, but still exhibiting a topographic high surface flanked by a steeper slope on one side and a less steep slope on the other side of the high (e.g., Figure 4c). An example of the Type-2 morphology includes the North Tanganyika-Rukwa RIZ (NTR-RIZ; 6.25°S, 30.5°E).

The topographic profile with Type-3 morphology is characterized by an elevated upper surface that extends from the axis of one of the interacting rift segments. This surface ramps steeply down to a lower elevation surface in the adjacent segment (e.g., Figure 4d). Type-3 morphology examples include the Southern Malawi–Shire (SMS-RIZ; 15.75°S, 34.75°E) and the Zambezi-Kafue (ZK-RIZ; 16°S, 28.5°E) RIZs. Finally, the Type-4 morphology features a considerably flat topographic relief profile that extends between the axis of the two interacting rift segments (Figure 4f). Examples of Type-4 morphology includes the Albertine–Rhino (AR-RIZ or BRIZ; 2.7°N, 31.4°E), and the Shire-Urema (SU-RIZ; 16.85°S, 35.35°E) RIZs.

However, we also observe another morphology type that has a form of Type-3 morphology but has more undulations on its ramp than the typical Type-3 morphology (Figure 4e). We dub this the 'Type-3-4' morphology. Except for the Upemba-Kundelungu RIZ (UK-RIZ; 9.15°S, 26.75°E), we commonly observe this morphology at the RIZs where active EARS segments overlap and overprint unreactivated Karoo rift basins. Examples include the Ruhuhu–Malawi (RM-RIZ; 10.75°S, 34.75°E), Maniamba–Malawi (MM-RIZ; 12. 5°S, 34.8°E), and Luama–Tanganyika (LT-RIZ; 5.9°S, 29.2°E) RIZs (Figure 4a). Along the Type-3-4 relief profile, the unreactivated Karoo basin extends from the ramp into the elevated part of the RIZ topographic relief profile.

Below, we focus on representative Type-1 to Type-4 RIZs along the WB-EARS and present observations of the pre-rift basement fabrics, faulting patterns, and axial drainage patterns and anomalies. We focus on the STR-RIZ, NTR-RIZ, SMS-RIZ, and AR-RIZ, due to the presence of accessible datasets that are relevant to our investigation. Due to the change in the RIZ geometry along the Tanganyika - Rukwa Rift cross-over zone (caused by along-strike change in the Tanganyika Rift trend), we separate the RIZ into a northern (NTR-RIZ) and southern (STR-RIZ) domain.

3.3. Representative Type-1 Morphology Rift Interaction Zone: The South Tanganyika-Rukwa Rift Interaction Zone (STR-RIZ)

The STR-RIZ is an overlapping-parallel divergent RIZ that is located between the Rukwa rift and the NW-trending southernmost segment of the Tanganyika rift (Figure 5a). The RIZ cross-over region, known as the Ufipa Horst, is essentially the uplifted basement horst between the Ufipa Fault footwall and the adjacent Tanganyika Rift (Figures 5a-c). This RIZ has recorded significant seismic activity, ranging from Mw<3.7 up to Mw7.4 (Figure 5a; Vittori et al, 1997).

3.3.1. Pre-rift Basement Fabrics and Rift Faulting in the STR-RIZ

The metamorphic foliation (i.e., 'basement fabrics') of the STR-RIZ basement revealed in the filtered aeromagnetic grid (Figures 5b-c), show dominant NW-SE trends with 148°±4.3 mean orientation (Figure 5d). Likewise, mapped faults (Figure 5c) within the RIZ show the same prominent trend, with a mean of 147°±3.2 (Figure 5e). On a larger-scale, we observe that the trends of the South Tanganyika Rift and its east bounding faults, as well as trends of the Rukwa Rift, its west bounding fault (Ufipa Fault), and the Kanda Fault (major fault in the RIZ; Figure 5f) are parallel to the dominant NW-SE trend of the basement fabrics. In this RIZ, we do not observe the presence of prominent cross-faulting that directly links the Rukwa and South Tanganyika Rift basins.

3.3.2. Axial Stream Morphology in the STR-RIZ

The axial streams within the RIZ (e.g., Kalambo(KIR), Momba (MR), Mfuizi (MfR), and R1 Rivers) generally flow parallel to the long-axis of the RIZ and are confined to narrow valleys that are bounded by steep fault scarps (Profile P1; Figures 5a and 5f). Downstream, the streams change course and flow into the interacting rift segments of Lake Tanganyika (in Tanganyika Rift) and Lake Rukwa (in the Rukwa Rift) (Figures 5a and 5g). The longitudinal profiles of representative axial streams (Kalambo and R1, which flow in opposite directions) show steepening of the profile with associated waterfalls (e.g. Kalambo Waterfall) along both the eastern and western flanks of the RIZ. Additionally, at the flanks of the RIZ, the streams commonly show a significant decrease in channel width and sinuosity relative to the upstream sections that extend well into the RIZ (e.g., Kalambo River, Figure 5g).

3.4. Representative Type-2 Morphology Rift Interaction Zone: The North Tanganyika-Rukwa Rift Interaction Zone (NTR-RIZ)

The NTR-RIZ has an overlapping-oblique divergent geometry, and is located between the northwestern tip of the Rukwa rift and the central segment of the Tanganyika rift (Figures 5a and 6a-b). Similar to the STR-RIZ, this northern RIZ has recorded significant seismic activity, including multiple Mw>5.0 events (Figure 5a).

3.4.1. Pre-rift Basement Fabrics and Rift Faulting in the NTR-RIZ

The basement fabrics of the NTR-RIZ show a dominant NW-SE trend observable on the aeromagnetic map (Figure 6a) with a mean of 139°±5.2 (Figure 6c). Also, the mapped faults in the RIZ (Figure 6b) show a prominent NW-trend with a mean of 137°±3.4 (Figure 6d), parallel to the basement fabrics. The mean trends of both the basement fabrics and faults in this RIZ are slightly oblique to those of the South Tanganyika - Rukwa RIZ, suggesting an anticlockwise deflection in the trend of the structures. This deflection is apparent in the fault map of the RIZs (Figure 5a). In the region of STR-RIZ to NTR-RIZ transition, two prominent NE-dipping fault scarps, Ifume and Nkamba Faults (Figures 5a, 6a-b) extend from the northernmost segment of Ufipa Fault System into the hanging wall of the SW-dipping Mahale Fault in the Tanganyika Rift. The basement exposures along the hanging walls of the scarps suggest an absence of large fault displacement or subsidence. The Nkamba River (NR in Figure 5a) extends from a watershed divide in the footwall of the Ufipa Fault, flows westward across the fault scarps into Lake Tanganyika (Figure 5a). However, more importantly, we note that the Nkamba and Ifume fault scarps show similarity of dip direction with the Rukwa Rift's NE-dipping Ufipa Fault, antithetic to the Tanganyika Rift's Mahale Fault.

Overall, the faults within the NTR-RIZ form a network that extends northwestwards from the tip of the Rukwa Rift and links up with faults along the eastern boundary of the Tanganyika Rift (Figure 6b). The RIZ-orthogonal topographic profiles (Figures 6e-g) show that at the NW tip of the Rukwa Rift, the basin is defined by a broad sediment-filled valley (smooth DEM surface texture) bounded by a low-gradient ramp that transitions to low-relief rift shoulders (Profile P2; Figure 6e). Further northwest, into the RIZ (Profile P3; Figure 6f), the basin morphology is characterized by multiple narrow sediment-filled troughs (narrow zones of smooth DEM surface texture) bounded by steep fault scarps and higher relief shoulders.

Proximal to the Tanganyika Rift (Profile P4; Figure 6g), the surface morphology of the RIZ is characterized by ubiquitous basement exposures with rare occurrence of significant sediment accumulation (rougher DEM surface textures). Two moderate magnitude (Mw>5.0) earthquakes in the NTR-RIZ show strike-slip kinematics with at least one nodal plane trending parallel to the mean fault trend and mean basement fabric trend (Figures 5a, 5d-e). However, near the Rukwa Rift tip, the events generally show oblique normal faulting (Figure 5a).

3.4.2. Axial Stream Morphology in the NTR-RIZ

The Type-2 topographic morphology of the NTR-RIZ (Figure 6h) features a central topographic-high flanked to the northwest (towards the Tanganyika Rift) by a steep escarpment, and to the southeast by a gentle slope that extends into the axis of the Rukwa Rift. Several humps and steps occur along the gentle slope and are collocated with the prominent NE-SW trending ridges (Figure 6h) that were formed by paleo-shorelines of Lake Rukwa (Figure 5a; Delvaux et al.,1998).

Within the RIZ, the axial streams (Kavuu (KR) and Luegele (LR) Rivers) diverge away from the central topographic-high (shared catchment region) and drain into the interacting rift basins (Figure 6h). The Luegele River flows northwest over a distance of ~55 km and drains into the Tanganyika Rift. The Luegele River steepens at ~28-30 km along the profile (Figure 6i) which is collocated with the steep escarpment that bounds the RIZ to the northwest. Within this steeper reach, the Luegele River is characterized by rapids (Luegele Rapids). We observe that although the channel width shows an abrupt decrease across the steep elevation gradient, the sinuosity index of the channel shows an increase on the downslope segment of the river (Figure 6i). The Kavuu River flows southeastwards from the RIZ and drains into the Rukwa Rift (Figure 5a). Although the channel extends over a longer distance (> 260 km) and transects a gently sloping topography (Figure 6i), the sinuosity and width of the channel show systematic variations. Two prominent anomalies are observable on the stream profile; these include an abrupt elevation step that is collocated with the Ilyandi Ridge and a change to a steep gradient at the Maimba Ridge (Figure 6i). Furthermore, we observe that the Kavuu River attains peak sinuosity index (~1.58) and channel width just upstream of two of the ridges, the Ilyandi Ridge and Rungwa Ridge. Each of these ridges is located just downstream of a prominent small lake (e.g., Lake Katavi) or swamp (Figure 5a). However, overall, the sinuosity of the axial streams is higher than those of the STR-RIZ.

3.5. Representative Type-3 Morphology Rift Interaction Zone: The South Malawi-Shire Rift Interaction Zone (SMS-RIZ)

The SMS-TZ covers the region extending from the southernmost tip of the N-S-trending Malawi Rift (i.e., the Zomba Graben) and the eastern margin of the NW-SE-trending Shire Rift Zone (i.e., Lower Shire Graben) (Figures 4a and 7a). Based on the overall trend of the Malawi Rift relative to the Shire Rift, we describe this cross-over region to be an overlapping oblique divergent transfer zone.

3.5.1. Pre-rift Basement Fabrics and Rift Faulting in the SMS-RIZ

To better understand the distribution of metamorphic basement fabrics and faulting in the SMS-RIZ (Figures 7b-c), we analyze the structures in the northern and southern parts of the Zomba Graben separately. The North Zomba Graben is distal to the Shire Rift, and the South Zomba Graben is proximal. The metamorphic fabrics of the North Zomba Graben are defined by curvilinear magnetic fabrics (Figure 7b) trending NNE-SSW (014°±4.1) (Figure 7di), parallel to the most prominent fault set (NNE-SSW, 011°±5.4; Figure 7dii). The secondary fault set (ENE-WSW, 073°) corresponds to the ENE linking faults along the NNE-trending border faults. This secondary fault set also corresponds to the trend of a prominent ENE strike-slip fault to which the Shire River channel is aligned (blue arrows in Figure 7a and c), and which also aligns with a basement dike lineament and offsets the basement metamorphic fabrics (Figure 7b).

In the South Zomba Graben, the metamorphic fabrics show bimodal trends with NNE-SSW (029°±3.9) and NW-SE (144°±4.2) sets (Figure 7ei) in which only the NNE set shows strong correspondence to a prominent fault set (Figure 7eii). The faults in the South Zomba Graben show multimodal trends with NNE-SSW (023°±4.6), NNW-SSE (164°±5.7), and ENE-WSW (079°) (Figure 7eii). The border faults of the South Zomba Graben generally follow basement fabrics, and although most of the intra-basinal faults and fractures crosscut the pre-rift fabrics, some segments locally follow the basement fabrics (Figure 7c).

The border faults of the Zomba Graben exhibit synthetic geometry mostly prominent in the south Zomba Graben. In the northern Zomba Graben, the intra-basinal faults dominantly trend NNE-SSW, parallel to the trend of the graben (Figure 7dii). In the south Zomba Graben, intra-basinal deformation is characterized by a cluster of faults/mega-fractures (breaching faults) generally trending NNW, and extend northwestward from the footwall of the Thyolo Fault, the border fault of the Shire Rift into the axis of the Zomba Graben (Figures 7a and 7c). The Thyolo Fault itself extends northwestwards, and in the region of overlap with the Zomba Graben, it rotates clockwise into a NNW-trend and continues as a mega-fracture through the axis of the Zomba Graben to link up with the western border fault system (Lisungwe Fault (LsF); Figures 7a and 7c).

3.5.2. Basin Morphology and Axial Stream Morphology in the SMS-RIZ

Within the SMS-RIZ (Figure 8a), the axial stream, the Shire River flows southward from Lake Malombe (Malombe Graben, Figures 8a-b), through the Zomba Graben and continues into the Shire Rift. The first-order trend of the Shire River is characterized by a systematic shift in the along-rift axial location of the stream. In the north (Malombe Graben), the river is located near the center of the rift (Figure 8c), whereas, in the North Zomba Graben, the river is located near the eastern border fault (Chingale Step Fault) (Figure 8d). From this location, the river deflects southwestwards such that its position is again at the rift axis within the central segment of the Zomba Graben (Figure 8e), but further south, is located near the western border fault of the graben (Lisungwe Fault, Figure 8f).

In addition, we observe that although the Malombe Graben is characterized by a graben (Figure 8b) to asymmetric graben (Figure 8c) geometries, the Zomba Graben presents an along-rift flip in the polarity of the basin morphology. In the North Zomba Graben the direction of the tilt of the basin is eastward (green arrow in Figure 8d) but flips to a westward tilt in the southern part of the rift (green arrow in Figures 8e-f). Essentially, the variations in the along-rift location of the Shire River are consistent with the along-rift change in the polarity of the basin and location of the dominant border fault.

We also observe that the morphology of the Shire River transitions from a relatively flat elevation profile upstream within the Malombe Graben and North Zomba Graben (Upper Shire River), through a steep profile in the South Zomba Graben (Middle Shire River), to a flat topography in the Shire Rift (Lower Shire River; Figure 8g). Along the Upper Shire River, the channel width mostly varies between 33 - 187 m with a sinuosity index of ~1.17 but decreases significantly to 15 – 130 m channel width and 1.04 sinuosity index in the Middle Shire River. Along the Lower Shire River, both the channel width and sinuosity index increase to values much higher than those of the Upper Shire River (60 – 215 m channel width and 1.28 sinuosity index; Figure 8g). Although the Upper Shire River is generally sinuous and curvilinear in geometry (Figure 8a), there exists two prominent localized zones of significantly high sinuosity patterns where the river exhibits anastomosing characteristics (anastomosing sections in Figures 8a and 8h). Whereas, the Middle Shire River exhibits major rectilinear and orthogonal geometries, some of which align with mapped fault and mega-fracture lineaments (e.g., Figure 8i). The Lower Shire River is highly sinuous throughout its length as it flows on the hanging wall of the Thyolo Fault (e.g., Figure 8j).

3.6. Representative Type-4 Morphology Rift Interaction Zone: The Albertine-Rhino Rift Interaction Zone (AR-RIZ, a.k.a. BRIZ)

The AR-RIZ is defined by the NNW-trending Butiaba RIZ (BRIZ) which is located between the NE-trending Albertine Rift to the south and the NE-trending Rhino Rift to the north (Figures

4a and 9a). This RIZ, also known as Pakwach Basin (Zwaan et al., 2016), is an underlapping parallel divergent RIZ.

3.6.1. Pre-rift Basement Fabrics and Rift Faulting in the BRIZ

Within the BRIZ, the basement fabrics show a prominent ENE-WSW trend (066°±9.3), with secondary NE-SW (033°±9.3) and E-W (094°±8.0) trends (Figure 9b). However, we observe that the BRIZ faults dominantly strike NNE-SSW (027±5.4°), oblique to the trend of the RIZ (Figure 9c). Faulting in the BRIZ is characterized by two main fault networks, both of which extend from two of the three prominent splay faults at the northern tip of the Bunia border fault of the Albertine Rift ("Splay-1, -2, & -3" in Figure 9a). The westernmost strand (Splay-1) connects to a network of short tightly clustered en-echelon faults, bounding the BRIZ to the west and southwest which extends northwards to link up with the western border fault of the Rhino Rift (Figure 9a). The central splay (Splay-2) continues north into the Ragem Fault, which appears to be the most prominent fault within the BRIZ. The Ragem Fault extend across the BRIZ into the footwall of the eastern border fault of the Rhino Rift. The easternmost splay (Splay-3) also extends across the BRIZ and is linked up with the Ragem Fault through the Panyango Fault. Overall, fault segments of Splay-3 appear to bound the BRIZ to the east and northeast (Figures 9a and 9e). In the Rhino Rift, the northern termination of the border fault systems occur at the NW-trending Precambrian Aswa Shear Zone (Figure 9a).

3.6.2. Basin Morphology and Axial Drainage Patterns in the BRIZ

The Albert Nile and Victoria Nile Rivers represent the major axial drainage systems of the Albertine Rift. However, the Albert Nile River is the primary axial drainage system that drains both the Albertine and Rhino Rifts, and the BRIZ between them (Figure 9a). Although the first-order trend of the Albert Nile River is generally sub-parallel to the trend of the RIZ, we observe that the along-rift locations of the river are collocated with the dominant border fault locations. The river flows northwards from the Lake Albert which is bounded by the border faults of the Albertine Graben (Figures 9a and 9d). In the BRIZ, the basin surface morphology shows a consistent northeastward-tilt, and the Albert Nile channel flows along the northeastern boundary of the RIZ (Figure 9a, 9e, and 9f). Within the Rhino Rift, the basin morphology is characterized by a southeastward-tilt (towards the Rhino Fault), and the Albert Nile flows along the hanging wall of the Rhino Fault (Figures 9a and 9g). Further north, closer to the rift termination at the Aswa Shear Zone, the river deflects towards the northwestern border fault (Figure 9a).

Overall, the entire longitudinal elevation profile of the Albert Nile River describes a relatively 'flat' topography with very wide segments (77 – 1,800 m width) characterized by large meanders and highly anastomosed morphology (Figure 10a-10e). We observe two broad partitions on the Albert Nile River morphology profile which consists of a northern and southern partition, separated by the Ragem Fault (Figures 10a and 10b). The southern partition consists of a single wide channel within a relatively narrower valley, featuring sparse anastomosing sections with wide stream branches (Figures 10a, 10b, 10c, 10d). The northern partition is characterized by a wider river valley of continuously anastomosing river segments with narrow stream branches and a high density of lakes (Figures 10a, 10b, 10e). The morphology of the northern partition of the river extends along most of the entire length of the Rhino Rift. On the hanging wall of the Ragem Fault, the river valley defines a roughly fault-parallel (NNE) trend, whereas, in the footwall of the fault, the river valley rotates into a fault-perpendicular (NNW) trend (Figure 10b).

Additionally, we observe an abrupt narrowing of the river channel across the Ragem Fault such that a wide lake (1.35 km-wide) ponds within the hanging wall of the fault and drains into a narrow (~300 m-wide) channel on the footwall of the fault (Figures 10a, 10b and 10d). Similarly, where the river crosses the Rhino, Panyango and Bunia Splay-3 faults, there is a change in the width of the river such that the wider sections occur on the hanging wall of the faults (Figures 10a, 10b-c, and 10e).

4. Discussion

4.1. A New and Broader Classification of Rift Interaction Zones

The existing geometrical classification of RIZs (Nelson et al., 1992) is useful, but is significantly lacking in that it does not encompass the variety of RIZ geometrical patterns that can be observed in modern continental rift systems. Also, the existing scheme is overly simplistic, and only considered the plan-view rift geometries (Nelson et al., 1992). The classification does not permit the analyses of complexities arising from multiphase extension with varying extension directions, and generally ignore the possible temporal evolution from one RIZ geometry into another. Here, we establish a unifying broader classification scheme that accommodates the plan-view geometries, polarity patterns (dip direction) of the large basin-bounding faults (border faults), and temporal transformation of the RIZ geometries (Figure 3).

Our new classification scheme features both paired rift RIZs (involving only 2 rift segments) and compound rift RIZs (involving >2 rift segments). Along the WB-EARS (Figure 4a), a few examples of the geometries shown in the new scheme include: Tip-to-tip collinear (Rukwa-North Malawi), Overlapping parallel divergent (Upemba-Kundelungu, Kundelungu–Luapula, South Tanganyika – Rukwa RIZs), Overlapping orthogonal divergent (Tanganyika-Mweru Wantipa RIZ), Overlapping oblique divergent (South Malawi-Shire and Luama–Tanganyika RIZs), Complex quadruple junction (Rukwa-Luangwa-North Malawi–Usangu RIZ).

In other continental rift systems, examples include Overlapping oblique divergent (Wetterau–Leine RIZ, European Cenozoic Rift System), Tip-to-tip oblique (South Viking–Witch Ground RIZ, North Sea Rift), Overlapping parallel divergent (Utsira High, North Sea Rift; Limagne–Bresse RIZ, European Cenozoic Rift System), Overlapping oblique convergent (Espaniola–San Luis RIZ, Rio Grande Rift), Overlapping parallel convergent (Albuqueque-Espaniola RIZ, Rio Grande Rift), Overlapping orthogonal divergent (Lower Rhine–Upper Rhine RIZ, European Cenozoic Rift System), and Underlapping parallel divergent (Upper Rhine-Bresse RIZ, European Cenozoic Rift System). All the overlapping parallel RIZs in the different continental rift settings examined show an x-offset rift axes separation <150 km, consistent with recent models (Neuharth et al., 2021) which suggest a limit of 300 km x-offset distance beyond which overlapping rift segments will likely not interact.

For each category of RIZ, we show the lateral extents of the cross-over region across which the breaching faults would develop and propagate. Also, we indicate the possible variations of the breaching distances across the cross-over regions, indicating the areas within the cross-over region where relatively shorter distances of fault propagation could facilitate breaching. We note that the configuration of some of the RIZ geometries suggest a possible temporal transformation from one geometry to another. For example, in paired RIZs, depending on the boundary conditions (e.g., underlapping distance, extension direction, inherited structures), with continued extension, unfaulted underlapping RIZs can evolve into an overlapping geometry or faulted underlapping geometry (see modelling results in Allken at al., 2012; Zwaan and Schreurs, 2020). Also, stress rotation between rifting episodes in multiphase rift settings can lead to the transformation of a paired RIZ geometry into a compound RIZ geometry; an example of which is the Turkana Depression (Fairhead, 1988; Emishaw et al., 2019; Morley, 2020; Wang et al., 2021).

Most numerical and analog models of rift linkage have been limited in scope because they only investigated parallel RIZs (underlapping and overlapping parallel RIZs, e.g., Acocella et al., 1999; Corti, 2004; Allken at al., 2011, 2012; Zwaan et al., 2016; Zwaan & Schreurs, 2017, 2020). An example of this limitation is the assumption that the Rukwa Rift represents a strike-slip strain transfer zone between the Tanganyika Rift and Malawi Rift (e.g., Zwaan & Schreurs, 2017) even though faults of the Rukwa Rift largely exhibit normal faulting kinematics (e.g., Morley et al., 1999; Morley, 2010; Lavayssière et al., 2019). Although models successfully reproduce the temporal transformation from a type of parallel RIZ into another, there remains the need to consider the wider variety of RIZ geometries as shown in our updated classification scheme. Overall, we clarify that the geometries shown in our new scheme are most representative of early-stage continental extension, as the complexity of reactivation and structural deformation increases with the progression of continental extension towards break-up.

In the following sections, within the framework of our RIZ geometrical classification for paired rift segments, we analyze and discuss the detailed characteristics of four representative RIZs along the Western Branch of the East African Rift System (WB-EARS, Figure 4a). Based on the structural and morphotectonic characteristics of each of the cross-over regions examined, we infer the likely stage of evolution of the RIZ, the patterns of breach faulting and the basement controls.

4.2. Rift Interactions at the South Tanganyika-Rukwa RIZ (STR-RIZ)

The STR-RIZ is an excellent example of Overlapping parallel divergent RIZ (Figures 2 and 5a). The prominent topographic-high and steep flank morphology of the Ufipa Horst (Type-1 morphology, Figure 4b), and the presence of waterfalls and rapids on the flanks (Figures 4b, 5f-g) suggest that the Ufipa Horst is actively uplifting along both of its flanks. This uplift is caused by both the flexural footwall uplift of the Ufipa Fault and eastern Tanganyika Rift faults, and a mantle-driven dynamic topography (Morley et al., 1999). However, even in the absence of the dynamic topography, the zone remains a horst block between the rift segments as shown in a published model of the Rukwa Rift (Morley et al., 1999).

Previous detailed study of the Rukwa Rift western border faults and Ufipa Horst faults (Heilman et al., 2019), and the clear correlation between the trends of basement metamorphic fabrics and faults within the block (Figures 5d and 5e) indicate an influence of the pre-rift basement fabrics on strain accommodation within the RIZ. In addition, the near-orthogonal orientation of the extension direction relative to the dominant basement fabric trends (Figures 5a and 5d-e) implies that the deformation of the RIZ could be accommodated by normal fault exploitation of the pre-rift basement fabrics. However, the complexity of kinematics of the deformation in the STR-RIZ is demonstrated by the prominence of Cenozoic oblique-normal and strike-slip faulting, with minor reverse faulting, possibly associated by local SHmin rotation (Delvaux et al., 2012; Lavayssière et al., 2019).

The mapped faults are parallel to the long axis of the Ufipa Horst with no major graben system connecting the Rukwa and Tanganyika Rifts (Figures 5b-c), and the crust which appears to have been intruded by magma, is relatively thicker than those of the flanking rifts (Hodgson et al., 2017; Lavayssière et al., 2019). The deformation of this RIZ is relatively less pronounced in comparison to the overlapping parallel NLNM-RIZ where the North Rukuru-Mwesia Rift and Henga Rift (NRR and HR in Figure 4a) represent a RIZ-parallel deformation of the cross-over region (Ring, 1995). Likewise, it is less pronounced in comparison to the deformation of the N-S-trending Limagne–Bresse RIZ by the NNW-trending Roanne-Forez graben system in the European Cenozoic Rift System (Dèzes et al., 2004). The breaching of the NLNM-RIZ and Limagne–Bresse RIZ is represented by the development of a cluster of narrower en-echelon rift basins within the cross-over zone, in which the rift cluster is parallel or sub-parallel to the interacting major rift segments. Whereas another overlapping parallel RIZ, the UK-RIZ (Figure 4a) presents a different case of breaching by a transverse structure (here in referred to as the “Lufira Fault, LF” in Figure 4a) with well-developed sediment-filled valley (Choubert et al., 1988) and a through-going axial stream (Lufira River) which physically link the Upemba and Kundelungu Rift basins. The N-S/NNW trend of the Lufira Fault is compatible with the SHmax rotation from NE-SW trend along the Upemba Rift to a N-S trend adjacent to the location of the Lufia Fault (Delvaux and Barth, 2010).

Therefore, the absence of any of the possible breaching structural patterns in the STR-RIZ suggests that the structural domain is partially deformed, and its breaching is not significant. The maximum separation distance between the Southern Tanganyika and Rukwa Rifts is <92 km (Figure 5f). Analog models (e.g., Zwaan and Schreurs, 2020) show that within a separation distance of <300 km, rift segments will interact. Thus, it is possible that the observed faulting within the RIZ (e.g., the Kanda and Kalambo-Mwimbi Fault Systems) is being driven by the interaction between the two rift segments, a previously reported dynamic mantle-related uplift within the Ufipa Horst (Morley et al., 1999; Heilman et al., 2019), or both. Overall, our preferred interpretation is that the STR-RIZ is a partially breached RIZ.

4.3. Rift Interactions at the North Tanganyika-Rukwa RIZ (NTR-RIZ)

The NTR-RIZ represents an overlapping oblique divergent RIZ. The shape of the topographic relief profile extending from North Tanganyika Rift to Rukwa Rift (Figure 6h) shows that, in contrast to the steeper NW flank of the NTR-RIZ (Tanganyika Rift), the SE flank (towards the Rukwa Rift) is characterized by a longer stretch of gently sloping topography. Along this long stretch of gentle topography, the first-order axial stream trends are parallel to the fault and basement fabric trends (indicating large-scale control of tectonic trends).

Multiple narrow troughs develop at the NW tip of the Rukwa Rift passing into the NTR-RIZ, delineating a young rift splay (Figures 6b and 6f). The Nkamba and Ifume fault scarps (at the STR-RIZ/NTR-RIZ transition zone) also show an association with this rift splay, indicated by their common NE-dip with the Rukwa Rift's Ufipa Fault and their eastern terminations in the footwall of the fault. The narrow troughs defined by the splays are bounded by actively propagating fault networks that extend northwest across the RIZ towards the eastern margins of the Tanganyika Rift. Thus, we interpret that the development of the Type-2 topographic relief shape across the NTR-RIZ is influenced by a progressive northwestward propagation of the NW tip of the Rukwa Rift towards the Tanganyika Rift (Figures 6b and 6e-g). Whereas the relative steepness of the northern flank of NTR-RIZ 2-D cross-over relief profile (Figure 6h) reflects an absence of pronounced southeastward propagation of rifting from the Tanganyika flank of the NTR-RIZ.

Several of the mapped faults in the NTR-RIZ extend from the tip of the Rukwa Rift into the interior of the RIZ. However, our interpretation of the northwestward propagation of the Rukwa Rift is supported by the anomalous clustering of earthquakes at the NW tip of the rift which indicates that active crustal deformation is partitioned to the southeastern section of the NTR-RIZ (Figure 5a; see clustering of relocated earthquakes in Lavayssière et al., 2019). Also, The Ifume and Nkamba Faults, representing the most-western splay of the NW Rukwa Rift tip exhibit moderate earthquake clustering (Figure 5a; Lavayssière et al-2019), indicating tectonic activity along the faults. Overall, the NTR-RIZ faults represent the RIZ breaching faults and are accommodating a mix of strike-slip and oblique-normal slip kinematics (Figures 5a, 6b, and 6f; Lavayssière et al., 2019). Among these faults, the Ifume and Nkamba Faults, and the NW-trending Mw5-hosting faults along-trend of the Kavuu River likely constitute the master strain transfer faults between the two rifts.

We interpret that the NTR-RIZ is a partially breached RIZ, in which the Rukwa Rift is the active propagator, and the north Tanganyika Rift is the ‘receiving’ segment. The active propagation of the Rukwa Rift tip is accompanied by splaying of the rift tip into multiple narrower troughs. The moderate magnitude strike-slip faulting (Mw>5) in the interior of the NTR-RIZ (Figure 5a) is compatible with the WNW-ESE regional extension direction and counterclockwise rotation of fault and basement fabric trends from the STR-RIZ to NTR-RIZ (Figures 5d-e, 6c-d). However, the presence of oblique normal faulting earthquakes near the Rukwa Rift tip (Figure 5a; Lavayssière et al 2019) possibly indicates local stress rotations in the RIZ (Morley, 2010). Local rotations of the SHmin orientation into fault-orthogonal trends have also been highlighted in the northern Malawi Rift (Kolawole et al., 2018) and southern Malawi (Williams et al., 2019). Overall, the alignment of fault trends and basement fabric trends (Figures 5d-e) suggest that at gross-scale, the RIZ breaching is associated with an exploitation of the inherited basement fabrics. With progressive strain accommodation along the breaching faults, well-developed fault-bounded breaching valleys with permanent fluvial system could develop, first along the Ifume and Nkamba faults, and subsequently, the faults along-trend of the Kavuu River. We note that the Ifume River which appear to extend from the Rukwa Rift into Lake Tanganyika only served as a temporary fluvial link between the two lakes during an ancient phase of overflooding of Lake Rukwa (Cohen et al., 2013).

We suggest that the 1st-order trends, flow directions, and longitudinal relief gradients of the RIZ-sourced axial streams in the NTR-RIZ indicate a dominant direction of the NTR-RIZ breaching. The Kavuu River (axial stream) originates near the termination zone of one of the splay troughs where the distal upstream segment of the stream shows generally smaller channel width and lower sinuosity (Figure 6i). Whereas further SW, within the Rukwa Rift, the river exhibits higher sinuosity and larger channel width. Other geomorphic features influencing the local shape of the axial stream profile are associated with lake-level fluctuations (Lake Rukwa paleo-shorelines; Figures 5a and 6i; Delvaux et al., 1998) which are controlled by coupled tectonics and paleoclimatic conditions (Delvaux et al., 2011).

4.4. Rift Interactions at the South Malawi-Shire RIZ (SMS-RIZ)

The border faults of the Zomba Graben are the southern continuation of the Malawi Rift border fault systems (Figure 7a). Thus, being the southernmost segment of the rift, the Zomba Graben represents the RIZ between the Malawi Rift and the Shire Rift. In the northern part of the Zomba Graben (distal to the Shire Rift), the intra-basinal and border faults are mostly parallel or sub-parallel and trend NNE, except for a few NE and ENE steps along the border faults (Figure 7a and 7dii). The alignment of the fault trends with the orientation of the pre-rift basement fabrics indicates a control of basement fabrics on fault geometries (Figure 7c, 7di and 7dii). Whereas basement fabrics and rift faulting in the South Zomba Graben appear to be relatively more complex, and the intra-basinal faults define an NNW-trending fault/mega-fracture cluster which is oblique to the NE-trend of the Zomba Graben and border faults (Figures 7a, 7c). This intra-basinal fault cluster extends NNW along the Lukhubula fault system in the footwall of the Thyolo Fault (Shire Rift active border fault) into the axis of the South Zomba Graben, exhibiting soft- and hard-linkage patterns with the Zomba Graben border faults (Lisungwe, Zomba, and Chingale Step Faults) and the North Zomba intra-basinal faults (Mlungusi and Mtsimukwe Faults).

The clockwise rotation of the northwestern tip of the Thyolo Fault from a NW trend to NNW trend appears to have been guided by a pre-existing basement shear zone (Figure 7c and inset; Morel, 1958), but is also well-oriented to be reactivated in the current ENE extension direction. Also, we note that although the breaching fault cluster in South Zomba Graben generally trend NNW, some of the segments locally crosscut- while others follow the basement fabrics (Figure 7c). Although the current extension direction (Figure 7a) is favorable for the reactivation of the NNE- and NW-trending border faults of the Zomba Graben and Shire Rift (Williams et al., 2019), the NNW-trend of the breaching fault cluster segments is even more optimally-oriented for reactivation in this regional stress field. Therefore, we infer that the breach faulting of the SMS-RIZ exhibits a partial control of pre-rift basement structures, but a stronger control of the tectonic extension direction. In summary, we suggest that there exists an appreciable structural linkage between the border faults of the Shire Rift and Zomba Graben, and that the deformation is compatible with the current stress field and in some places, associated with local exploitation of pre-rift basement fabrics.

The consistency between the along-rift alternation of basin polarity (basin tilt direction, e.g., Mack et al., 2006) and the along-rift changes in the location of the main axial stream (Shire River) indicates the first-order control of rift structure on axial drainage pattern in the Zomba Graben (Figures 8b-f). The alignment of a segment of the Shire River with a collocated buried fault and dike (white arrows in Figures 7a and 7c) may also indicate a secondary structural control on the stream geometry. However, more importantly, the morphology of the RIZ relief profile (south-facing ramp/step; Type-3 morphology) indicates a unidirectional southward flow pattern across the RIZ (Figure 8g), along-trend of which the pre-rift basement is broadly exposed at the rift floor and is flanked to the east and west by the graben border faults (Figures 8a and 8i). This zone of exposed basement on the rift floor is collocated with the Middle Shire River where the axial stream longitudinal profile becomes steeper and is dominated by waterfalls, rapids, narrowed channel, and fracture-controlled stream segments (Figures 8g and 8i).

The waterfalls and rapids mostly cluster in the northern part of the area of the rift-floor basement exposure where the Shire River follows the limb of a plunging fold structure (see Figures 7b-c, and 8a and 8g). At a large-scale, there is no observable basement lithologic contact (Figures 7b-c) cross-cutting the river channel at the location of the waterfalls, however, it is possible that locally, lithologic contacts influence their development. Overall, the mega-scale 'topographic step' in the Middle Shire River, itself represents the most prominent knickpoint along the entire course of the Shire River. We suggest that the waterfalls likely developed as the stream attempts to adjust to a new longitudinal drainage profile (supported by observations in Bloomfield, 1965; Dulanya, 2017). Therefore, these observations all together, indicate that although the SMS-RIZ is breached, the breaching is most likely a recent event.

The southern Malawi Rift evolved through the episodic southward propagation of the Malawi Rift (Scholz et al., 2020), subsequently leading to its tectonic interaction with the eastern sub-basin (Lower Shire sub-basin) of the Shire Rift Zone. The North Zomba Graben is dominated by paleo-lake sedimentary deposits (Matope Beds and associated lacustrine clays) of Neogene age or younger which directly overlie the Precambrian basement unconformity surface, and are overlain by the alluvial sediments of the Shire River (Bloomfield and Garson, 1965; Thomas et al 2009; Lyons et al 2015; Dulanya, 2017; Wedmore et al 2020). This shallow paleo-lake (or swamp) developed within a structural-low land area (fault-bounded?) surrounded by basement uplifts from which sediments were sourced into the lake (Dulanya, 2017). In essence, the paleo-lake was restricted to the south by an elevated basement area, which separated the lake from the Shire Rift. Based on paleo-environmental reconstruction and consideration of likely provenance of the paleo-lake sediments, it was concluded that linkage of the Upper and Lower Shire River segments (i.e., linkage of the Zomba Graben and Shire Rift depositional environments) is a 'recent' feature (Dulanya, 2017). The observations of a previously restricted depocenter in the North Zomba Graben are consistent with our analyses, emphasizing that the present-day location of the South Zomba Graben (Middle Shire River segment) must have been an elevated basement region in pre-Quaternary times. Thus, the progressive brittle deformation, erosion, and subsidence of the uplifted cross-over region (in the Quaternary) facilitated the continuous south-directed flow of the axial stream (Shire River) from the Lakes Malawi and Malombe, through the south Zomba area, into the Lower Shire sub-basin of the Shire Rift.

We suggest that the breaching of the SMS-RIZ is facilitated by both the NW-NNW propagation of the Thyolo Fault (and the Lukhubula Fault System in its footwall) and the concurrent southward propagation of the Zomba Graben border faults, largely guided by the current extension direction. An early-rift localization of significant intra-basinal strain in the Zomba Graben has been highlighted but is inferred to be possibly controlled by a deeper lower-crustal mechanical heterogeneity along the rift axis (Wedmore et al., 2020). However, the basement fabrics (which represent exhumed lower-crustal structures) do not show the presence of a discrete pre-rift terrain boundary along the rift axis (Figure 7b); rather the fabrics show a north-plunging fold structure. Although, the large fold structure extends across the entire rift width, the large-scale aeromagnetic character of the basement fabrics changes across the western border fault (Lisungwe Fault) and more significantly across the eastern border fault system (Chingale Step and Zomba Faults) (Figures 7b-c; also see Nyalugwe et al., 2019a, 2020). Most of the length of the Lisungwe Fault (LsF) appear to have propagated along a boundary of contrasting basement fabrics (NE-SW and WNW-ESE fabrics in the hanging wall, NW-SE and N-S fabrics in the footwall). Thus, the prominent mechanical weaknesses of the exhumed basement occur primarily along the border fault zones and not the intrabasinal domain of the Zomba Graben. Therefore, we suggest that this early-stage intra-basinal strain localization in the Zomba Graben can also be explained by the recent breaching of the RIZ and migration of strain into the axis of the Zomba Graben through the breaching fault/mega-fracture clusters.

4.5. Rift Interactions at the Albertine–Rhino RIZ (AR-RIZ, a.k.a. BRIZ)

The Butiaba Rift Interaction Zone (BRIZ) represents the RIZ between the Albertine and Rhino Rifts. The BRIZ is bounded by a tight cluster of short en-echelon faults to the southwest and relatively longer fault segments to the southeast and northeast (Figure 9a). Although the basement fabrics show a multimodal trend (Figure 9b), a secondary NNE-trending set is parallel to the dominant fault trend (Figure 9c). We observe that two major breaching fault systems extend from the NW border fault of the Albertine Rift (Bunia Fault), across the BRIZ, and soft-link or hard-link with the border faults of the Rhino Rift. These two systems include the tight cluster of short en-echelon faults that appear to link up with the western Luku border fault of the Rhino Rift, and a system of fault splay consisting of three 'large' fault strands that extend towards the southern tip and footwall of the Rhino border fault of the Rhino Rift (Figure 9a). These BRIZ breaching fault systems are sub-orthogonal to the crustal stretching direction, are locally parallel to a pre-rift fabric trend, and oblique to the trend of the BRIZ (Figure 9a and 9c). Also, the extension direction is moderately oblique to the rift trends, consistent with analog modelling results (Zwaan et al., 2016). Overall, these geometrical relationships suggest that the brittle deformation of the BRIZ exploited the basement fabrics in an oblique rifting tectonic setting.

The axial stream longitudinal profile is very flat in this region, and the river itself is characterized by generally large channel widths (Figure 10a), suggesting a low energy equilibrated axial stream. The morphology of this axial stream profile relative to those of the other representative RIZs analyzed in this study is quite unique and indicative of the evolutionary stage of the RIZ. Seismic reflection imaging of a part of the BRIZ that is proximal to the Albertine Rift reveals ~2 km sedimentary fill (Simon et al., 2017), indicating a relatively significant basin subsidence in the RIZ. This magnitude of subsidence in the BRIZ is important, considering that prior to the structural deformation and subsidence across a RIZ, the cross-over region must have been an elevated basement area (see analog models in Zwaan et al., 2016). These observations lead us to infer that the Albertine – Rhino RIZ is indeed a breached RIZ, and that any paleo-intervening basement-high is faulted (footwall blocks of Ragem Fault and Bunia Fault Splay-3) and buried, and the axial stream now simply flows across its own floodplain.

We suggest that the Ragem Fault (northern splay-2 of the Bunia Fault) and the splay-3 of the Bunia Fault represent the master strain transfer faults in the BRIZ. However, it is much likely that as continental extension progresses, the present structure of the RIZ will continue to evolve. Recent seismicity in the RIZ suggests continued reactivation of the breaching faults.

If the Ragem Fault continues to propagate further northward into the footwall of the Rhino Rift, prominent overlapping geometries may develop between the Rhino and Albertine Rifts. The change in the channel geometry, channel width, and the partitioning of morphology anomalies of the of the Albert Nile River across the major RIZ faults (Ragem, Panyango, and Splay-3; Figures 10a-e), and recent earthquakes (Figure 9a), demonstrate that the BRIZ faults are still active. The findings also support a continued structural control on the large-scale axial stream morphology in a breached RIZ along young continental rifts.

4.6. The Stages of Rift Linkage in Non-Magmatic Continental Rift Interaction Zones

4.6.1. Evolutionary Stages of Rift Segment Interaction and Linkage across RIZs

To assess the stage of breaching of a RIZ (i.e., stage of linkage of the associated interacting rift segments), we consider: 1) the presence or absence of faults extending from one rift segment to the other rift segment, and 2) the presence of an established physical linkage of the depositional environments of the two rifts (i.e., are the basins open to each other?). Based on the observed fault patterns in the representative RIZs, the extents and flow directions of the associated axial streams, and long-wavelength topographic relief shapes, we present four possible sequential stages of RIZ breaching and rift linkage in active continental rift systems (left panel of Figure 11). These stages include 1) unbreached, 2) partially breached, 3) recently breached, and 4) breached RIZs. Further, based on the observed directionality of axial stream flow and rift-related sediment accumulation zones around the analyzed RIZs, we present an idealized stratigraphic evolution of the sedimentary stratigraphy of the RIZs (middle and right panels of Figure 11).

Prior to rift linkage, the intervening RIZ is essentially a relatively elevated basement region with steep flanks relative to the axes of the interacting rift basins (unbreached RIZ separating unlinked rift segments, Stage-1; Figure 11a). At this stage, the axial streams of the two rifts with sources in the cross-over region are not linked, such that a bi-directional pattern of sediment dispersal (2-D perspective along cross-over profile) from the RIZ into the rift basins will likely dominate. However, with the progressive lateral propagation of the rift tips, the breaching faults extend further into the RIZ, grabens and half-grabens begin to localize within the RIZ, and with continued erosion of the elevated areas, localized zones of subsidence and sediment accumulation begin to extend from the rift tips into the RIZ. Thus, an unbreached RIZ may evolve into a narrowed cross-over basement-high with fault networks that extend between the interacting rift tips but in which a through-going well-developed rift valley is yet to develop across the RIZ, a stage which we describe as a "partially breached RIZ" (partially linked rifts, Stage-2; Figure 11b). The NTR-RIZ, and the Luano-Kafue RIZ (LK-RIZ) exhibit characteristics that demonstrate this stage of rift linkage. As a note of caution, we emphasize that the cross-over topographic relief geometries of a Stage-2 RIZ is likely strongly dependent on the directionality of propagation of the RIZ breaching and the spatial variation of basement erodibility.

With continued propagation of the breaching faults and deepening of grabens within the deforming RIZ, the rift bounding faults of the interacting rift segments establish connection and one or more well-developed rift valleys are established across the RIZ. As the rift linkage creates a continuous rift valley floor connecting the interacting rift basins, a reversal of the antecedent axial streams sourced from the RIZ may occur, resulting in the development of a common axial stream that flows unidirectionally between the newly-linked rift segments. At this initial stage of successful establishment of rift linkage, we refer to the RIZ as a "recently breached RIZ" (recent rift linkage, Stage-3; Figure 11c). The SMS-RIZ (Figure 4a) exhibits characteristics that can be interpreted to represent this stage of rift linkage. We clarify that 'recent' as used in the context of "recently breached RIZs" is qualitative, primarily relevant to modern active continental rift environments.

The transition from Stage 2 to Stage 3 facilitates the evolution of the interacting rifts from hydrologically closed basins to open ones as their depositional systems become linked (e.g., Gawthorpe and Leeder, 2000). Also, we highlight the possible prominence of capturing and/or reversals of antecedent axial streams flowing into the interacting rift basins as the RIZ cross-over region transitions from Stage 2 to Stage 3. However, it should be noted that apart from strain rates on breaching faults, how quickly a Stage-2 RIZ (partially breached) transitions into Stage 3 can be significantly determined by basement structure and lithological heterogeneity, which often impact the rates of fluvial erodibility and drainage divide mobility patterns within the uplifted cross-over region (e.g., Annandale, 1995; Zondervan et al., 2020). Also, the fluvial erodibility and drainage divide mobility within the deforming RIZ prior to linkage, and the rate of sediment filling in the interacting basins at the Stage 3 will potentially influence the transition from one stage to another.

Finally, with the continued coalescence of the linked breaching and border fault systems of the interacting rifts, the RIZ cross-over topography becomes progressively worn down by the axial drainage system and its transverse streams as unidirectional flow of the axial stream dominates. Also, the axial stream longitudinal profile attains the form of a low energy equilibrated axial drainage system. We refer to this stage as "breached RIZ" (Figure 11d).

Thus, in humid continental rift settings where sedimentation rates are keeping up with strain rates on faults, the breaching of RIZs and structural linkage of interacting rift segments are important for persistent drainage network connectivity and sediment transport between the interacting rift segments.

We note the common occurrence of the Type-3-4 morphology at the RIZs separating active EARS and unreactivated Mesozoic Karoo rifts (e.g., Figure 4e). The exception is the UK-RIZ where the interacting rifts although are EARS segments, contain Mesozoic Karoo sedimentary rocks (Choubert et al., 1988). Thus, we infer that the Type-3-4 morphology indicates a RIZ that is breached, in which the breaching may or may not have occurred in the most recent phase of extension. However, more importantly, the morphology represents a breached RIZ in which the axial stream has not yet equilibrated. Along the WB-EARS, where a Type-3-4 cross-over profile connects a failed Mesozoic rift with an overlapping active EARS segment, the Mesozoic rift basin is often located in the elevated part of the profile which is in the rift flank of the active rift and is explainable by the flexural uplift of the flanks of the active rift segment. Therefore, due to the uplift of the rift flank, the sedimentary or volcanic rift-fill of the failed rift will generally undergo erosion and incision by streams as the deposits are reworked into the linked actively subsiding rift basin. However, if a Type-3-4 cross-over morphology is observed across an RIZ between two active rift segments, this may indicate an imbalance of sediment supply rate relative to strain rate between the two linked active rift segments, thus, creating an overfilled basin in one segment, and an underfilled one in the other.

We emphasize that defining the breach stage of an active RIZ solely by the cross-over topographic morphology only could be misleading. For example, although the Zambezi-Kafue RIZ (ZK-RIZ) exhibits a Type-3 morphology, and the axial stream (Kafue River) flows unidirectionally across the RIZ, there no evidence of graben or half graben development along the axial stream valley. Thus, in this case, the fluvial linkage of the Kafue and Zambezi Rifts is likely not related to a structural breaching of the RIZ. We speculate that the development of Type-3 morphology across the ZK-RIZ is related to Holocene-age dynamic topographic uplift in the vicinity of the Kafue Rift (Daly et al., 2020) possibly resulting in the sediment overfilling-to-spill in the rift, or a combination of this and a partial structural breaching of the ZK-TZ.

The simplified models presented in Figure 11 summarize our observations along the WB-EARS, and idealizations in aspects for which we do not have direct observations (e.g., buried subsurface stratigraphy of breached RIZs). The models assume 1) a humid continental setting, 2) orthogonal extension, 3) the erodibility of the pre-rift basement is relatively uniform, 4) sediment supply into the interacting rift basins keeps up with strain rates on faults, and 5) no significant influence of dynamic topography within the deforming RIZs. Although our models are based on regions of active early-stage (stretching phase) continental rifting in which at least one of the interacting rift pairs is active, the observations are relevant for buried rift interaction zones in ancient rift settings. Our study suggests that for a given directionality of breaching, paired RIZs that are not fault-bounded or are fault-bounded on only one flank should exhibit a distinct long-wavelength 2-D topographic relief shapes. When the assessment of the long-wavelength 2-D topographic relief shape across the RIZ is combined with analyses of the breaching fault patterns, the stage of RIZ breaching can be inferred (Figure 11). Therefore, given the assumptions made on the models, the 2-D topographic profiles across an unbreached RIZ exhibit a shape that is similar to Type-1 morphology (depending on if the RIZ is fault-bounded or not), and profiles across an RIZ that is already breached or is in the final stages of breaching should exhibit shapes similar to Type-3, Type-3-4, or Type-4.

The overlapping parallel RIZs along the WB-EARS generally have a lateral rift-orthogonal separation distance of ≤100 km, consistent with recent analog models (Allken at al., 2011, 2012; Zwaan and Schreurs, 2020) which suggest an upper limit of 300 km separation distance, below which rift segments will likely not interact. However, the deformation patterns in various overlapping parallel RIZs in natural rift settings show that this RIZ geometry may be unique, in that the attainment of breaching may involve the development of 1.) cross-faulting that connects the interacting rift segment tips, 2.) cross-faulting that extend across the intervening horst block (i.e., flanks of interacting segments), and/or 3.) localization of a cluster of narrower en-echelon rift basins (i.e., subsidiary rift basins) within the horst block. However, in the case of the development of such subsidiary rift basins (e.g., NLNM-RIZ in Figure 4a, and Limagne–Bresse RIZ), the breaching of the RIZ must involve the structural connectivity of the subsidiary basins with at least one of the interacting rift segments and transport of the sediments between both.

Since the linkage of interacting rift segments is manifested in the physical linkage of their intra-basinal and/or border fault segments, we hypothesize that post-linkage, interacting rifts may show a record of accelerated strain and subsidence across the breached RIZ (Figures 11d and 12; Gawthorpe and Leeder, 2000). Studies have shown that the linkage and coalescence of propagating fault segments often lead to increased strain accommodation and basin subsidence rates along the newly linked faults (e.g., Gupta et al., 1998; Gawthorpe and Leeder, 2000; Taylor et al., 2004; Cowie et al., 2005). For example, in the Whakatane Graben, New Zealand, the post-linkage displacement rate of the major normal faults increased by up to threefold (Taylor et al., 2004). The unavailability of high-resolution data on fault displacement rates at the representative WB-EARS RIZs analyzed in our study makes it currently difficult to test this hypothesis. Therefore, there is a need to better understand the significance of the temporal variations of breaching fault displacement rates for the evolution of RIZs. Overall, we emphasize that post-linkage, coalesced rift basins may preserve a buried record of paleo-RIZs that indicate the location of an initial phase of separated rift segments, progressive breaching of the intervening zones, and subsequent linkage of the segments (Figure 12).

4.7. Lateral Rift Segment Propagation and Directionality of RIZ Breaching

4.7.1. What Drives the Lateral Propagation and Interaction of Continental Rift Segments?

At the larger rift system-scale, continental rift propagation is driven by gravitational stresses and extension gradients imposed by rotational and orthogonal plate extension, assuming a homogenous continental crust (Corti et al., 2007; Mondy et al., 2018; Molnar et al., 2018; Zwaan and Schreurs, 2020). Also, rotational rifting may play important roles in driving rift segment propagation during late-stage rift settings where transitional crust dominates (e.g., the Afar region, Kidane et al., 2003; Zwaan and Schreurs, 2020). However, at the relatively less understood segment-scale of rift propagation in juvenile rift settings, our study suggests that anomalous earthquake clustering at the rift tips indicates local stress concentrations at the propagating rift tips (e.g., NTR-RIZ, Figure 5). Another example of this is the anomalous clustering of earthquakes at the northern and southern tips of the Turkana Rift (Musila et al., 2020). We argue that similar to the mechanics of fracture propagation (e.g., Kranz, 1979), such stress concentrations at and ahead of the tips of active rift segments play important roles in driving the propagation of breaching faults from the rift tip into the associated RIZ. Further, we find that the geometries of the propagating breaching faults are modulated by both the extension direction and inherited (pre-rift) basement fabrics. We speculate that the focusing of magmatism at rift interaction zones (e.g., Rungwe, Toro-Ankole, and Kivu Volcanic Provinces in Figure 4a; Njinju et al., 2019a,b), in combination with magma-driven faulting, reflects an important contribution of magmatism to lateral rift propagation into deforming RIZs (Heilman et al., 2019).

4.7.2. Directional Propagation of RIZ Breaching and Rift Linkage

The lateral separation geometry of interacting continental rift segments (underlap/overlap angles and distance) determines if and how they will interact spatially (e.g., Tentler and Acocella, 2010; Zwaan et al., 2016; Zwaan and Schreurs, 2020; Neuharth et al., 2021). Thus, with continued tectonic extension, an isolated rift segment may progressively propagate laterally until its 'breaching distance' (distance from another rift segment) is small enough to permit interaction and development of breaching faults in the RIZ cross-over area. Our observations at the representative non-magmatic RIZs and observations along other segments of the East African Rift System reveal three distinct styles of rift propagation associated with RIZ breaching (Figures 12a-b). In one case, we observe that only one of two interacting rift segments acts as the propagating segment (i.e., the 'propagator') such that the other 'non-propagating' segment represents the 'receiver', demonstrating a unidirectional style of RIZ breaching and rift linkage (Figure 12a). For example, in the NTR-RIZ (Figure 6), the Rukwa Rift represents the propagator, and the Tanganyika Rift represents the receiver.

In another case, we find evidence that suggests that both interacting segments propagated towards one another, indicating a bi-directional style of RIZ breaching (Figure 12a). An example of bi-directional RIZ breaching is the SMS-RIZ (Figures 7 and 8). In a third case, strain localizes within the interior of the RIZ as a narrower rift basin which propagates outwards to link with the major interacting rift segments (Figure 12b). An example of this intra-RIZ outward breaching is the Turkana Depression which represents the zone of interaction between the Main Ethiopian Rift and the Kenya Rift (Wang et al., 2021). Within the Turkana Depression RIZ, the Turkana Rift appears to have developed as a single coherent tectonic element that localizing most of the intra-RIZ strain and is facilitating rift linkage across the Turkana Depression (Knappe et al., 2020; Musila et al., 2020).

Also, it is important to note that in areas of multiphase rifting where a younger rift segment may propagate towards an older failed rift segment, the younger active rift represents a propagator, and the 'inactive' (or partially active) older rift segment largely represents a receiver. Further, we suggest that the geometrical configuration of certain RIZ classes (Figure 3) promote the dominance of unidirectional breach propagation over bi-directional propagation. For example, overlapping oblique and overlapping orthogonal RIZs would almost always experience unidirectional breach propagation. Whereas overlapping and underlapping parallel RIZs may accommodate both unidirectional and bi-directional breach propagation patterns.

4.7.3. Rift-Tip Structures and Rift-Flank Interactions

Models of interaction between parallel rift pairs (i.e., parallel RIZs) have demonstrated how the obliquity or orthogonality of extension direction can influence the patterns of rift-tip interactions and geometry of breaching faults in homogeneous media, and in the presence of a connecting pre-existing fault (e.g., Acocella et al., 1999; Aanyu and Koehn, 2011; Zwaan et al., 2016; Zwaan and Schreurs, 2017, 2020). Model results and the natural examples examined in our study show that the breaching of RIZs is facilitated by more complex patterns of structural deformation that link the interacting rift basins.

On a large-scale, we find that RIZ breaching is commonly facilitated by propagating rift-tip (e.g., in tip-to-tip collinear, and underlapping RIZs) and/or rift-flank deformation (e.g., in some overlapping oblique and parallel divergent RIZs). Along the WB-EARS, we observe that propagating rift-tips are characterized by 1) rift splay creating a pattern of smaller and narrower graben and/or half-grabens (e.g., rift bifurcations, rift trifurcations etc.), 2) rotation of the propagating border fault tip, and/or 3) network of fault clusters, that extend into deforming RIZs. An example of rift-flank deformation is the breaching of the UK-RIZ, NLNM-RIZ, and SMS-RIZ (Figures 4a and 12a). Whereas examples of rift splay include splay troughs at the NW Rukwa Rift tip, bifurcation of the SE Rukwa Rift tip, trifurcation (or greater) of the NW Luama Rift tip, bifurcation of the northern Edward Rift tip, splay faulting at the northern Albertine Rift tip (Figures 4a and 13a). An example of border fault tip rotation is the clockwise rotation of the NW tip of the Thyolo border fault in the SMS-RIZ. Also, examples of RIZ breaching by fault cluster networks include the BRIZ and SMS-RIZ (Figures 7a and 9a).

We suggest that rift splay and border fault rotation are analogous to the geometries of fault networks that have been observed at the laterally propagating fault tips (e.g., Kim et al., 2004; Perrin et al., 2016; Phillips et al., 2019). Although rift splay was previously presented as a type of rift segment geometry (Nelson et al., 1992), we argue here that rift splays and border fault rotation at rift tips represent genetic characteristics of the lateral propagation of rift segment tips. Thus, such structures, although not the RIZ itself, could suggest the termination zone of a rift segment, or that a propagating rift segment is approaching an interaction zone with another rift segment. Numerical models show the development of rift tip splays and/or border fault rotation at RIZs in areas of lateral propagation and interaction of rift segments (e.g., Zwaan et al.,2016; Zwaan and Schreurs, 2020; Neuharth et al., 2021).

Thus, the preservation of the rift-tip structures highlighted in this study within the syn-rift sequences of composite rift basins (i.e., coalesced segmented rifts) may provide insight into previous rift-tip termination zones and zones of interaction with another rift segment prior to linkage. For example, the buried bifurcation zone in the central Malawi Rift (vicinity of the Likoma-Lipichilli Horst; Specht and Rosendahl, 1989) is collocated with the inferred earlier termination zone of the northern Malawi Rift during the long-term southward propagation of the Malawi Rift (Scholz et al; 2020).

An example of buried border fault rotation zone is in the central Tanganyika Rift where the rift is segmented across the Kavala Island Ridge - a RIZ which was breached and buried as seen in seismic interpretations (Wright et al., 2020). The vicinity of the Kavala Island Ridge (Kalemie area, central Tanganyika Rift) shows a relatively lower tectonic extension relative to the northern Ruzizi-Kigoma and southern Marungu-Mpulungu sub-segments (Wright et al., 2020); indicating that the central Tanganyika area is a paleo-RIZ between the northern and southern sub-segments prior to the breaching and subsidence of the Kavala Island ridge. The Rwenzori RIZ between the Edward and Albertine Rifts show both well-developed bifurcation and border fault rotation patterns (Koehn et al., 2008).

At zones of rift slays, it appears that at least one of the splay branches (splay trough) may eventually 'fail' while one or more branches continue to localize most of the tectonic strain and facilitate a successful linkage with the interacting rift segment. For example, the Songwe Trough of the SE Rukwa Rift bifurcation has localized greater strain and breaching of the Rukwa–North Malawi RIZ (Mbozi block) than the Musangano Trough (Heilman et al., 2019). Additionally, the Malombe Graben of the Southern Malawi Rift bifurcation is a better-developed bifurcation branch than the Makanjira Trough as evidenced by the continuation of the rift valley floor, axial stream linkage (Shire River), and localization of a major lake (Lake Malombe) along the Malombe Graben (Figures 7a, 8a and 8c; see also Dulanya, 2017).

Overall, our analyses show that although RIZs may differ in both their geometries and evolutionary stages, there exist distinct long-wavelength 2-D cross-over relief profile geometries that are unique to each of the evolutionary stages within a given erodibility structure, breaching propagation directionality, strain rate, and sediment-supply rate across the RIZ. We envision that our observations in this study provide predictive models for the geometry and temporal evolution of paleo-RIZs preserved in the stratigraphic record of mature continental rifts and passive margin basins. However, we acknowledge that further refinement of these models should be undertaken with additional studies of both ancient and modern systems.

4.8 Implications for Early-Stage Continental Rift Growth in East Africa

Along the eastern Africa rift zones analyzed in this study, based on the long wavelength cross-over relief morphology, fluvial isolation/linkage of interacting rifts, and the general breaching fault patterns at the RIZs, we find that at least 60 % of the RIZs exhibit characteristics of breaching (Figures 13a and 13b). The unbreached and partially breached RIZs account for up to ~37 % of the RIZs. We characterize all magmatic RIZs as "breached" because of the lithospheric-scale deformation associated with magmatism. Several of the Mesozoic rift segments (pre-EARS) show characteristics of breaching across the RIZs (fault connectivity and proximity/overlapping of rift-fill e.g., Kariba-Zambezi, Ruhuhu–Malawi, Maniamba-Malawi, Luangwa-Zambezi, and Shire-Zambezi RIZs; Figure 13a). The development and lateral propagation of the Cenozoic rift segments have facilitated their linkage with the Mesozoic rift segments (Delvaux, 1989). Overall, we note that the northern regions of the WB-EARS and the southern regions of the EB-EARS appear to be dominated by breached RIZs, whereas the rift segments further south show more of partially breached, recently breached, and unbreached RIZs (Figure 13a). The apparent southward and southwest-ward increase in the occurrence of unbreached, partially breached, and recently breached RIZs reflects the proposition of an active southwest-ward propagation of the East African Rift System (Daly et al., 2020).

Cenozoic continental extension in the EARS initiated ~40 Ma (Boone et al., 2019), and its Western Branch (WB-EARS) evolved ~25 Ma (Roberts et al., 2012), such that by the Middle Miocene to Pliocene, most of the rift segments had been established (Simon et al., 2017; Scholz et al., 2020). However, the predominance of breached RIZs along these juvenile branches of the East African Rift System (Figure 12a), suggest that the early-stage establishment of the EARS segments is associated with considerable RIZ breaching and rift linkage. This is supported by previous observation of early linkage of rift faults along the East African Rift System (Morley, 1999).

Although the EARS is actively growing, the early-development of most of its segments is consistent with observations of early-stage rapid establishment of segments in the East Greenland rift system (i.e., within the first 20 % of rift life; Rotevatn et al., 2018). Therefore, we propose that the continued southward and southwest-ward growth of the EARS (Ebinger, 1989; Chorowicz, 2005; Daly et al., 2020; Zwaan and Schreurs, 2020; Ngalamo et al., 2020) will likely record continued episodes of lateral propagation of the rift tips, linkage across the RIZs, intensified deformation and burial of previously breached (paleo-RIZs) and recently breached RIZs.

4.9 Outstanding Questions

It was suggested that small scale tensile fractures are possible analogs of actively propagating continental rift segments (Nelson et al., 1992). Heilman et al. (2019) further speculated that the laterally propagating rift tips are zones of stress concentration with a distinct 'process zone', and that RIZs are areas of overlap between the process zones of rift segments that are in proximity of one another. While the geometries and aspects of the kinematics of micro-scale fractures may appear similar to those of continental rifts, it is not yet known if the mathematical solutions for fracture tip propagation are applicable and relevant to the scale of rift basins.

Studies in different continental rift settings have highlighted that RIZs, magmatic focusing, and rift linkage are often collocated (e.g., Aldrich, 1986; Ebinger, 1989; Nelson et al., 1992; Acocella et al., 1999; Wilson, 1999; Muirhead et al., 2015; Heilman et al., 2019). However, since the RIZ breaching faults are relatively younger and often not as well developed as the major faults of the interacting rift segments, questions remain on this proposed association. Further, we raise another question on the relationship between the successful branches of a rift splay and the localization of RIZ magmatism. We observe that the higher strain Songwe Trough of the SE Rukwa Rift bifurcation hosts the Rungwe Volcanic Province (Figure 4a; Heilman et al., 2019), whereas the Toro Ankole Volcanic Province is in the Lake George Graben of the northern Edward Rift bifurcation (Figures 4a and 13a). Also, there is a need to better understand the mechanisms that facilitate magmatic focusing into RIZs with thick crusts in young continental rift settings (e.g., lower crustal intrusions in South Tanganyika – Rukwa RIZ; Hodgson et al., 2017). In addition, there is a need to better understand the absence of magmatism in breached RIZs where no surface or deeper magmatism have been observed (e.g., Albertine - Rhino Rift's BRIZ). Future studies should also investigate the influence of short-wavelength dynamic topography on RIZ evolution.

Although magmatic RIZs generally show elevated geothermal anomalies, local elevated geothermal gradients and heat flow is also observed to localize at active non-magmatic RIZs (e.g., SMS-TZ, Njinju et al., 2019a; Walker Lane-Northern Great Basin Transfer Zone, Faulds et al., 2010). Thus, interesting questions remain on the relationship between the temporal evolution of RIZs and the associated crustal thermal state in active rift settings. Future studies should investigate the significance of RIZs and their breach state for geothermal system development in active rift settings.

There is a relatively faster crustal stretching rate (2.7 - 2.9 mm/yr) near the partially-breached Tanganyika-Rukwa RIZ compared to the 1.5 mm/yr crustal stretching rate near the recently-breached South Malawi-Shire RIZ (Saria et al., 2014). However, since the tectonic strain is typically distributed across several faults within an active rift basin, and rift segment propagation being facilitated by stress concentrations at the rift tip, there remain outstanding questions on the factors that preferentially localize tectonic stresses at the rift tips, away from the rift axis. Also, we suggest that there is a need to better understand the partitioning of seismic versus aseismic strain across actively deforming RIZs, the relevance of these modes of strain accommodation in magmatic and non-magmatic RIZs and implications for rift linkage.

Conclusions

We review rift interaction zone (RIZ) geometries, and in the magma-poor, juvenile western Branch of the East African Rift System, we investigated the stages of rift linkage and the associated physiographic, structural, and broad-scale sedimentation patterns. We examine representative non-magmatic RIZs in the region and explore the relationships between the breaching faults, basement structure, and axial stream patterns. Our main results are:

1.) A new and broader rift interaction zone classification that encompasses a wider range of plan-view RIZ geometries and dip polarity of the interacting border faults.

2.) Although RIZs may differ in both their geometries and evolutionary stages, there exist distinct long-wavelength 2-D topographic relief geometries, directionality of axial stream flow, and breaching fault patterns that characterize RIZs at the various stages of rift linkage.

3.) These stages include unbreached RIZ (associated with unliked rifts), partially breached RIZ (partially linked rifts), recently breached RIZ (recently linked rifts), and breached RIZ (linked rifts). Post linkage of the rift segments, a coalesced rift forms, and the zone of rift linkage which is buried beneath the younger rift-fill is referred to as a paleo-RIZ.

4.) At deforming RIZs, breaching may propagate in a single direction i.e., unidirectional (distinct propagator and receiver segments), or in a bi-directional manner (both interacting segments act as propagators and receivers), which may also modulate the cross-over relief shape. Also, we find that breaching may propagate outwards from the RIZ in the form of a narrow intra-RIZ subsidiary rift basin.

5.) Depending on the RIZ geometry, breaching is commonly facilitated by rift-flank deformation and/or distinct rift-tip structures. Propagating rift-tip structures observed in the study areas include rift splay, border fault rotation (rift-tip rotation), and fault cluster networks.

6.) The lateral propagation of the RIZ breaching faults at the rift tips and flanks, facilitated by local stress concentrations, is modulated by both the extension direction and inherited basement structures.

7.) At least 60 % of the RIZs along the western, southwestern, and southeastern branches of the EARS exhibit breached rift interaction zone characteristics, indicating the early linkage of the rift segments. In addition, unbreached and partially breached RIZs are largely located in the southern and southwestern parts of the rift system, likely indicating a progressive lateral rift propagation and coalescence to the south and southwest of the rift system.

Our findings offer a broader insight into the geometrical complexity and structural evolution of rift interaction zones, and provide first-order predictions of large-scale sedimentation patterns of humid early-stage continental rift environments. Further, the models proposed in this study provide testable hypotheses for linking rift architecture and patterns of early-stage (stretching phase) rift sedimentation applicable to ancient rift basins. However, we acknowledge that further refinement of these models should be undertaken with additional studies of both ancient and modern rift systems.

Acknowledgements

We thank the South African Development Community (SADC) for providing the Tanzania aeromagnetic dataset used in this study. Thanks to Geological Survey of Malawi for providing the 2013 aeromagnetic datasets used in this study. None of the authors have a conflict of interest to declare. We also thank the editor Atle Rotevatn, reviewers Christopher Morley, Jack Williams, and three additional anonymous reviewers for their constructive comments that have helped to improve the quality of the manuscript. Also, thanks to Frank Zwaan for useful comments on the preprint of this paper (available on https://eartharxiv.org).

Data Availability

The Global Multi-Resolution Topography (GMRT) dataset used in this study is public domain and is freely available through the GeoMapApp (Ryan et al., 2009). The southern Malawi Total Magnetic Intensity (TMI) dataset is archived at the Interdisciplinary Earth Data Alliance (IEDA) at doi:10.1594/IEDA/324860 (Nyalugwe et al., 2019b).

References

Aanyu, K. and Koehn, D., 2011. Influence of pre-existing fabrics on fault kinematics and rift geometry of interacting segments: analogue models based on the Albertine Rift (Uganda), Western Branch-East African Rift System. Journal of African Earth Sciences, 59(2-3), 168-184.

Acocella, V., Faccenna, C., Funiciello, R. and Rossetti, F., 1999. Sand-box modelling of basement-controlled transfer zones in extensional domains. Terra Nova-Oxford, 11(4), pp.149-156.

Aldrich, M.J., 1986. Tectonics of the Jemez Lineament in the Jemez Mountains and Rio Grande Rift. J. Geophys. Res. 91, 1753–1762.

Allen, P.A., 2008. From landscapes into geological history. Nature, 451(7176), 274-276.

Allken, V., Huismans, R.S. and Thieulot, C., 2011. Three ‐ dimensional numerical modeling of upper crustal extensional systems. Journal of Geophysical Research: Solid Earth, 116(B10).

Allken, V., Huismans, R.S. and Thieulot, C., 2012. Factors controlling the mode of rift interaction in brittle ‐ ductile coupled systems: A 3D numerical study. Geochemistry, Geophysics, Geosystems, 13(5).

Annandale, G.W., 1995. Erodibility. Journal of hydraulic research, 33(4), 471-494.

Arkani-Hamed, J. (1988). Differential reduction-to-the-pole of regional magnetic anomalies. Geophysics, 53(12), 1592–1600. https://doi.org/10.1190/1.1442441.

Barnes, J.B., Densmore, A.L., Mukul, M., Sinha, R., Jain, V. and Tandon, S.K., 2011. Interplay between faulting and base level in the development of Himalayan frontal fold topography. Journal of Geophysical Research: Earth Surface, 116(F3).

Behn, M.D., Lin, J., 2000. Segmentation in gravity and magnetic anomalies along the U.S. east coast passive margin; implications for incipient structure of the oceanic lithosphere. J. Geophys. Res. 105 (11), 25769–25790.

Bloomfield, K., and Garson, M. S. 1965. The geology of the kirk range – Lisungwe valley area. Bulletin of the Geological Survey of Malawi 17, Government Printer, Zomba.

Boone, S.C., Kohn, B.P., Gleadow, A.J., Morley, C.K., Seiler, C. and Foster, D.A., 2019. Birth of the East African Rift System: Nucleation of magmatism and strain in the Turkana Depression. Geology, 47(9), 886-890.

Bosworth, W., 1985. Geometry of propagating continental rifts. Nature, 316(6029), 625-627.

Braile, L., Keller, G., Wendlandt, R., Morgan, P., & Khan, M. (2006). Chapter 5 The east african rift system. Continental Rifts:Evolution, Structure, Tectonics Developments in Geotectonics.

Childs, C., Holdsworth, R. E., Jackson, C. A.-L., Manzocchi, T., Walsh, J. J. & Yielding, G. (eds) 2017. The Geometry and Growth of Normal Faults. Geological Society, London, Special Publications, 439, 79–107.

Chorowicz, J., 2005. The east African rift system. Journal of African Earth Sciences, 43(1-3), pp.379-410.

Choubert, G., Faure-Muret, A., Chanteux, P., Roche, G., Simpson, E.S.W., Shackleton, L., Ségoufin, J., Seguin, C. and Sougy, J., 1988. International geological map of Africa. Scale 1: 5 000 000, Commission for the Geological Map of the World (CGMW), Unesco, Paris.

Cochran, J.R., Martinez, F., 1988. Evidence from the northern Red Sea on the transition from continental to oceanic rifting. Tectonophysics 153 (1–4), 25–53.

Cohen, A. S., Bocxlaer, B. V., Todd, J. A., Mcglue, M., Michel, E., Nkotagu, H. H., … Delvaux, D. (2013). Quaternary ostracodes and molluscs from the Rukwa Basin (Tanzania) and their evolutionary and paleobiogeographic implications. Palaeogeography, Palaeoclimatology, Palaeoecology, 392, 79–97.

Collanega, L., Corti, G., Breda, A., Massironi, M. and Keir, D., 2020. 3D Extension at Plate Boundaries Accommodated by Interacting Fault Systems. Scientific Reports, 10(1), 1-12.

Corti, G. (2012). Evolution and characteristics of continental rifting: Analog modeling-inspired view and comparison with examples from the East African Rift System. Tectonophysics, 522, 1–33.

Corti, G., Cioni, R., Franceschini, Z., Sani, F., Scaillet, S., Molin, P., Isola, I., Mazzarini, F., Brune, S., Keir, D. and Erbello, A., 2019. Aborted propagation of the Ethiopian rift caused by linkage with the Kenyan rift. Nature communications, 10(1), 1-11.

Cowie, P.A., Underhill, J.R., Behn, M.D., Lin, J. and Gill, C.E., 2005. Spatio-temporal evolution of strain accumulation derived from multi-scale observations of Late Jurassic rifting in the northern North Sea: A critical test of models for lithospheric extension. Earth and Planetary Science Letters, 234(3-4), 401-419.

Daly, M.C., Chorowicz, J. and Fairhead, J.D., 1989. Rift basin evolution in Africa: the influence of reactivated steep basement shear zones. Geological Society, London, Special Publications, 44(1), 309-334.

Daly, M.C., Green, P., Watts, A.B., Davies, O., Chibesakunda, F. and Walker, R., 2020. Tectonics and Landscape of the Central African Plateau, and their implications for a propagating Southwestern Rift in Africa. Geochemistry, Geophysics, Geosystems, 21, p.e2019GC008746.

Delvaux, D., 1989. The Karoo to Recent rifting in the western branch of the East-African Rift System: A bibliographical synthesis. Mus. roy. Afr. centr., Tervuren (Belg.), Dépt. Géol. Min., Rapp. ann, 1990 (1991), 63-83.

Delvaux, D. and Barth, A., 2010. African stress pattern from formal inversion of focal mechanism data. Tectonophysics, 482(1-4), pp.105-128.

Delvaux, D., Kervyn, F., Vittori, E., Kajara, R.S.A. and Kilembe, E., 1998. Late Quaternary tectonic activity and lake level change in the Rukwa Rift Basin. Journal of African Earth Sciences, 26(3), pp.397-421.

Delvaux, D., Kervyn, F., Macheyeki, A. S., & Temu, E. B. (2012). Geodynamic significance of the TRM segment in the East African Rift (W‐Tanzania): Active tectonics and paleostress in the Ufipa plateau and Rukwa basin. Journal of Structural Geology, 37, 161–180. https://doi.org/10.1016/j.jsg.2012.01.008

Dèzes, P., Schmid, S.M. and Ziegler, P.A., 2004. Evolution of the European Cenozoic Rift System: interaction of the Alpine and Pyrenean orogens with their foreland lithosphere. Tectonophysics, 389(1-2), 1-33.

Drury, S. A. (2001). Image interpretation in geology, 3rd Edition, Blackwell Science Inc., Malden, MA.

Dulanya, Z., 2017. A review of the geomorphotectonic evolution of the south Malawi rift. Journal of African Earth Sciences, 129, pp.728-738.

Ebinger, C.J., 1989. Tectonic development of the western branch of the East African rift system. Geological Society of America Bulletin, 101(7), pp.885-903.

Ebinger, C.J. (2012). Evolution of the Cenozoic East African rift system. *Regional Geology and Tectonics: Phanerozoic Rift Systems and Sedimentary Basins*, 132–162.

Emishaw, L. and Abdelsalam, M.G., 2019. Development of Late Jurassic‐Early Paleogene and Neogene‐Quaternary Rifts Within the Turkana Depression, East Africa From Satellite Gravity Data. Tectonics, 38(7), 2358-2377.

Fairhead, J.D., 1988. Mesozoic plate tectonic reconstructions of the central South Atlantic Ocean: the role of the West and Central African rift system. Tectonophysics, 155(1-4), 181-191.

Faulds, J.E. and Varga, R.J., 1998. The role of accommodation zones and transfer zones in the regional segmentation of extended terranes. Geological Society of America Special Papers, 323, pp.1-45.

Faulds, J., Coolbaugh, M., Bouchot, V., Moek, I. and Oguz, K., 2010, April. Characterizing structural controls of geothermal reservoirs in the Great Basin, USA, and Western Turkey: developing successful exploration strategies in extended terranes. In World Geothermal Congress 2010, 11-p.

Fossen, H., SchulRIZ, R.A., Rundhovde, E., Rotevatn, A. and Buckley, S.J., 2010. Fault linkage and graben stepovers in the Canyonlands (Utah) and the North Sea Viking Graben, with implications for hydrocarbon migration and accumulation. AAPG bulletin, 94(5), 597-613.

FriRIZ, H., Abdelsalam, M., Ali, K. A., Bingen, B., Collins, A. S., Fowler, A. R., et al. (2013). Orogen styles in the East African Orogen: A review of the Neoproterozoic to Cambrian tectonic evolution. Journal of African Earth Sciences, 86, 65–106.

Gawthorpe, R.L. and Leeder, M.R., 2000. Tectono-sedimentary evolution of active extensional basins. Basin Research, 12(3-4), 195-218.

Gupta, S., Cowie, P.A., Dawers, N.H. and Underhill, J.R., 1998. A mechanism to explain rift-basin subsidence and stratigraphic patterns through fault-array evolution. Geology, 26(7), pp.595-598.

GTK Consortium (2012), Explanation of the geology of sheets NA-36-1 and NA-36-5 (Arua and Pakwach) 1:250,000, Uganda. Department of Geological Survey and Mines (DGSM), Entebbe. 115p.

Hans Nelson, C., Karabanov, E.B., Colman, S.M. and Escutia, C., 1999. Tectonic and sediment supply control of deep rift lake turbidite systems: Lake Baikal, Russia. Geology, 27(2), pp.163-166.

Heron, P.J., Peace, A.L., McCaffrey, K.J.W., Welford, J.K., Wilson, R., van Hunen, J. and Pysklywec, R.N., 2019. Segmentation of rifts through structural inheritance: Creation of the Davis Strait. Tectonics, 38(7), pp.2411-2430.

Hodgson, I., Illsley ‐ Kemp, F., Gallacher, R. J., Keir, D., Ebinger, C. J., & Mtelela, K. (2017). Crustal structure at a young continental rift: A receiver function study from the Tanganyika Rift. Tectonics, 36, 2806–2822.

Hovius, N. (1998). Controls on sediment supply by large rivers. In: Relative role of eustasy, climate and tectonism in continental rocks: Tulsa, Oklahoma. (Ed. By Shanley, K.W. & McCabe, P. J). SEPM Special Publication, 59, 2–16.

Jackson, C.A.L., Gawthorpe, R.L., Carr, I.D. and Sharp, I.R., 2005. Normal faulting as a control on the stratigraphic development of shallow marine syn-rift sequences: the Nukhul and Lower Rudeis Formations, Hammam Faraun fault block, Suez Rift, Egypt. Sedimentology, 52(2), pp.313-338.

Katumwehe, A.B., Abdelsalam, M.G. and Atekwana, E.A., 2015. The role of pre-existing Precambrian structures in rift evolution: The Albertine and Rhino grabens, Uganda. Tectonophysics, 646, pp.117-129.

Katumwehe, A.B., Abdelsalam, M.G., Atekwana, E.A. and Laó-Dávila, D.A., 2016. Extent, kinematics and tectonic origin of the Precambrian Aswa Shear Zone in eastern Africa. Gondwana Research, 34, pp.241-253.

Kidane, T., Courtillot, V., Manighetti, I., Audin, L., Lahitte, P., Quidelleur, X., Gillot, P.Y., Gallet, Y., Carlut, J. and Haile, T., 2003. New paleomagnetic and geochronologic results from Ethiopian Afar: Block rotations linked to rift overlap and propagation and determination of a~ 2 Ma reference pole for stable Africa. Journal of Geophysical Research: Solid Earth, 108(B2).

Kim, Y.S., Peacock, D.C. and Sanderson, D.J., 2004. Fault damage zones. Journal of structural geology, 26(3), pp.503-517.

Koehn, D., Aanyu, K., Haines, S. and Sachau, T., 2008. Rift nucleation, rift propagation and the creation of basement micro-plates within active rifts. Tectonophysics, 458(1-4), 105-116.

Kolawole, F., Atekwana, E.A., Laó-Dávila, D.A., Abdelsalam, M.G., Chindandali, P.R., Salima, J. and Kalindekafe, L., 2018. Active deformation of Malawi rift's north basin Hinge zone modulated by reactivation of preexisting Precambrian Shear zone fabric. Tectonics, 37(3), pp.683-704.

Kranz, R.L., 1979, February. Crack-crack and crack-pore interactions in stressed granite. In International Journal of Rock Mechanics and Mining Sciences & Geomechanics Abstracts (Vol. 16, No. 1, pp. 37-47). Pergamon.

Lambiase, J.J. and Bosworth, W., 1995. Structural controls on sedimentation in continental rifts. Geological Society, London, Special Publications, 80(1), 117-144.

La Rosa, A., Pagli, C., Keir, D., Sani, F., Corti, G., Wang, H. and Possee, D., 2019. Observing Oblique Slip During Rift Linkage in Northern Afar. Geophysical Research Letters, 46(19), 10782-10790.

Lavayssière, A. J., Drooff, C. J., Ebinger, C. J., Gallacher, R. J., Illsley-Kemp, F. J., Oliva, S. J., & Keir, D. J. (2019). Depth Extent and Kinematics of Faulting in the Southern Tanganyika Rift, Africa. Tectonics, 38(3), 842–862. doi: 10.1029/2018tc005379.

Lazarus, E. D., and Constantine, J. A. (2013). Generic theory for channel sinuosity. Proceedings of the National Academy of Sciences, 110(21), pp.8447-8452.

Lyons, R. P., Scholz, C. A., Cohen, A. S., King, J. W., Brown, E. T., Ivory, S. J., et al. (2015). Continuous1.3-million-year record of East African hydroclimate, and implications for patterns of evolution andbiodiversity. Proceedings of the National Academy of Sciences of the United States of America, 112(51),15,56815,573.

Ma, G. Q., Du, X. J., Li, L. L., & Meng, L. S. (2012). Interpretation of magnetic anomalies by horizontal and vertical derivatives of the analytic signal. Applied Geophysics, 9(4), 468–474. https://doi.org/10.1007/s11770-012-0350-4.

Mack, G.H., Seager, W.R., Leeder, M.R., Perez-Arlucea, M. and Salyards, S.L., 2006. Pliocene and Quaternary history of the Rio Grande, the axial river of the southern Rio Grande rift, New Mexico, USA. Earth-Science Reviews, 79(1-2), pp.141-162.

Mardia, K. V., and Jupp, P. E., 2009. Directional statistics. Vol. 494, John Wiley & Sons, West Sussex, England.

Molnar, N.E., Cruden, A.R. and Betts, P.G., 2018. Unzipping continents and the birth of microcontinents. Geology, 46(5), pp.451-454.

Mondy, L.S., Rey, P.F., Duclaux, G. and Moresi, L., 2018. The role of asthenospheric flow during rift propagation and breakup. Geology, 46(2), pp.103-106.

Molnar, N.E., Cruden, A.R. and Betts, P.G., 2019. Interactions between propagating rifts and linear weaknesses in the lower crust. Geosphere, 15(5), 1617-1640.

Morley, C.K., 1999, Aspects of Transfer Zone Geometry and Evolution in East African Rifts, in C.K. Morley ed., Geoscience of Rift Systems—Evolution of East Africa: AAPG Studies in Geology No. 44, 161–171.

Morley, C.K., 2020. Early syn-rift igneous dike patterns, northern Kenya Rift (Turkana, Kenya): Implications for local and regional stresses, tectonics, and magma-structure interactions. Geosphere, 16(3), 890-918.

Morley, C. K., Cunningham, S. M., Harper, R. M. and Wescott, W. A. (1992). Geology and geophysics of the Rukwa rift, East Africa. Tectonics, 11(1), pp.69-81.

Morley, C.K., Nelson, R.A., Patton, T.L. and Munn, S.G., 1990. Transfer zones in the East African rift system and their relevance to hydrocarbon exploration in rifts. AAPG bulletin, 74(8), 1234-1253.

Muirhead, J.D., Kattenhorn, S.A. and Le Corvec, N., 2015. Varying styles of magmatic strain accommodation across the East African Rift. Geochemistry, Geophysics, Geosystems, 16(8), pp.2775-2795.

Muirhead, J. D., Wright, L. J., & Scholz, C. A. (2019). Rift evolution in regions of low magma input in East Africa. Earth and Planetary Science Letters, 506, 332–346.

Musila, M., Ebinger, C. J., Mwangi, S., Kianji, G., Ayele, A., Mariita, N., Bastow, I. D., Bendick, R. O., 2020. Kinematics of linkage between the Main Ethiopian and Eastern rifts in the Turkana Depression. AGU Fall Meeting abstract #T024-0004.

Nelson, R.A., Patton, T.L. and Morley, C.K., 1992. Rift-segment interaction and its relation to hydrocarbon exploration in continental rift systems (1). AAPG bulletin, 76(8), pp.1153-1169.

Neuharth, D., Brune, S., Glerum, A., Heine, C. and Welford, J.K., 2021. Formation of continental microplates through rift linkage: Numerical modelling and its application to the Flemish Cap and Sao Paulo Plateau. Geochemistry, Geophysics, Geosystems, p.e2020GC009615.

Ngalamo, J.F.G., Kolawole, F., Sobh, M. and Atekwana, E.A. (2020). Partitioning of Extension at the Propagating Tips of Continental Rifts: Insights from the Central and East African Rift Systems. AGU Fall Meeting Abstract #T028-06.

Njinju, E.A., Kolawole, F., Atekwana, E.A., Stamps, D.S., Atekwana, E.A., Abdelsalam, M.G. and Mickus, K.L., 2019a. Terrestrial heat flow in the Malawi Rifted Zone, East Africa: Implications for tectono-thermal inheritance in continental rift basins. Journal of Volcanology and Geothermal Research, 387, p.106656.

Njinju, E.A., Atekwana, E.A., Stamps, D.S., Abdelsalam, M.G., Atekwana, E.A., Mickus, K.L., Fishwick, S., Kolawole, F., Rajaonarison, T.A. and Nyalugwe, V.N., 2019b. Lithospheric structure of the Malawi rift: implications for magma‐poor rifting processes. Tectonics, 38(11), pp.3835-3853.

Nyalugwe, V.N., Abdelsalam, M.G., Atekwana, E.A., Katumwehe, A., Mickus, K.L., Salima, J., Njinju, E.A. and Emishaw, L., (2019a). Lithospheric structure beneath the Cretaceous Chilwa Alkaline Province (CAP) in southern Malawi and northeastern Mozambique. Journal of Geophysical Research: Solid Earth, 124(11), pp.12224-12240.

Nyalugwe, V.; Abdelsalam, M.; Atekwana, E.; Katumwehe, A.; Mickus, K.; Salima, J.; Njinju, E. and L. Emishaw, (2019b). 2013 Total Magnetic Intensity (TMI) gridded aeromagnetic data of southern Malawi 34 45 E – 36 00 E and 14 45 S and 16 15 S (investigator Mohamed Abdelsalam). Integrated Earth Data Applications (IEDA). doi:10.1594/IEDA/324860.

Nyalugwe, V.N., Abdelsalam, M.G., Katumwehe, A., Mickus, K.L. and Atekwana, E.A., 2020. Structure and tectonic setting of the Chingale Igneous Ring Complex, Malawi from aeromagnetic and satellite gravity data: Implication for Precambrian terranes collision and Neogene-Quaternary rifting. Journal of African Earth Sciences, 163, p.103760.

Pagli, C., Yun, S.H., Ebinger, C., Keir, D. and Wang, H., 2019. Strike-slip tectonics during rift linkage. Geology, 47(1), pp.31-34.

Perrin, C., Manighetti, I. and Gaudemer, Y., 2016. Off-fault tip splay networks: A genetic and generic property of faults indicative of their long-term propagation. Comptes Rendus Geoscience, 348(1), pp.52-60.

Phillips, T.B. and McCaffrey, K.J., 2019. Terrane Boundary Reactivation, Barriers to Lateral Fault Propagation and Reactivated Fabrics: Rifting Across the Median Batholith Zone, Great South Basin, New Zealand. Tectonics, 38(11), pp.4027-4053.

Ring, U., 1995. Tectonic and lithological constraints on the evolution of the Karoo graben of northern Malawi (East Africa). Geologische Rundschau, 84(3), 607-625.

Roberts, E.M., Stevens, N.J., O'Connor, P.M., Dirks, P.H.G.M., Gottfried, M.D., Clyde, W.C., Armstrong, R.A., Kemp, A.I.S. and Hemming, S., 2012. Initiation of the western branch of the East African Rift coeval with the eastern branch. Nature Geoscience, 5(4), pp.289-294.

Rosendahl, B.R., 1987. Architecture of continental rifts with special reference to East Africa. Annual Review of Earth and Planetary Sciences, 15, p.445.

Rotevatn, A., Kristensen, T.B., Ksienzyk, A.K., Wemmer, K., Henstra, G.A., Midtkandal, I., Grundvåg, S.A. and Andresen, A., 2018. Structural inheritance and rapid rift-length establishment in a multiphase rift: The East Greenland rift system and its Caledonian orogenic ancestry. Tectonics, 37(6), pp.1858-1875.

Ryan, W. B. F., S.M. Carbotte, J. Coplan, S. O'Hara, A. Melkonian, R. Arko, R.A. Weissel, V. Ferrini, A. Goodwillie, F. Nitsche, J. Bonczkowski, and R. Zemsky (2009), Global Multi-Resolution Topography (GMRT) synthesis data set, Geochem. Geophys. Geosyst., 10, Q03014.

Roberts, E.M., Stevens, N.J., O'Connor, P.M., Dirks, P.H.G.M., Gottfried, M.D., Clyde, W.C., Armstrong, R.A., Kemp, A.I.S. and Hemming, S., 2012. Initiation of the western branch of the East African Rift coeval with the eastern branch. Nature Geoscience, 5(4), pp.289-294.

Saria, E., Calais, E., Stamps, D.S., Delvaux, D. and Hartnady, C.J.H., 2014. Present-day kinematics of the East African Rift. Journal of Geophysical Research: Solid Earth, 119(4), pp.3584-3600.

Simon, B., Guillocheau, F., Robin, C., Dauteuil, O., Nalpas, T., Pickford, M., Senut, B., Lays, P., Bourges, P. and Bez, M., 2017. Deformation and sedimentary evolution of the Lake Albert Rift (Uganda, East African rift system). Marine and Petroleum Geology, 86, pp.17-37.

Scholz, C.A., Shillington, D.J., Wright, L.J., Accardo, N., Gaherty, J.B. and Chindandali, P., 2020. Intrarift fault fabric, segmentation, and basin evolution of the Lake Malawi (Nyasa) Rift, East Africa. Geosphere, 16(5), 1293-1311.

Soreghan, M.J. and Cohen, A.S., 1996. Textural and compositional variability across littoral segments of Lake Tanganyika: the effect of asymmetric basin structure on sedimentation in large rift lakes. AAPG bulletin, 80(3), pp.382-408.

Soreghan, M.J., Scholz, C.A. and Wells, J.T., 1999. Coarse-grained, deep-water sedimentation along a border fault margin of Lake Malawi, Africa; seismic stratigraphic analysis. Journal of Sedimentary Research, 69(4), pp.832-846.

Specht, T.D. and Rosendahl, B.R., 1989. Architecture of the Lake Malawi rift, east Africa. Journal of African Earth Sciences (and the Middle East), 8(2-4), pp.355-382.

Taylor, S.K., Bull, J.M., Lamarche, G. and Barnes, P.M., 2004. Normal fault growth and linkage in the Whakatane Graben, New Zealand, during the last 1.3 Myr. Journal of Geophysical Research: Solid Earth, 109(B2).

Thomas D. S. G., Bailey, R., Shaw, P. A., Durcan, J. A., & Singarayer, J. S. (2009). Late Quaternaryhighstands at Lake Chilwa, Malawi: Frequency, timing and possible forcing mechanisms in the last 44 ka.Quaternary Science Reviews, 28, 526–539.

Tiercelin, J.J., Soreghan, M., Cohen, A.S., Lezzar, K.E. and Bouroullec, J.L., 1992. Sedimentation in large rift lakes: example from the Middle Pleistocene—Modern deposits of the Tanganyika Trough, East African Rift System. Bull. Centres Rech. Explor.-Prod. Elf Aquitaine, 16, pp.83-111.

Vittori, E., Delvaux, D. and Kervyn, F., 1997. Kanda fault: A major seismogenic element west of the Rukwa Rift (Tanzania, East Africa). Journal of Geodynamics, 24(1-4), pp.139-153.

Wang, L., Maestrelli, D., Corti, G., Zou, Y. and Shen, C., 2021. Normal fault reactivation during multiphase extension: Analogue models and application to the Turkana depression, East Africa. Tectonophysics, p.228870.

Wedmore, L., Biggs, J., Williams, J., Fagereng, A., Dulanya, Z., Mphepo, F. and Mdala, H. (2020). Active fault scarps in southern Malawi and their implications for the distribution of strain in incipient continental rifts. Tectonics, 39, e2019TC005834.

Westerhof, A.B., Härmä, P., Isabirye, E., Katto, E., Koistinen, T., Kuosmanen, E., Lehto, T., Lehtonen, M.I., Mäkitie, H., Manninen, T. and Mänttäri, I. (2014). Geology and geodynamic development of Uganda with explanation of the 1:1,000,000 scale geological map. Geological survey of Finland.

Williams, J.N., Fagereng, Å., Wedmore, L.N., Biggs, J., Mphepo, F., Dulanya, Z., Mdala, H. and Blenkinsop, T., 2019. How do variably striking faults reactivate during rifting? Insights from southern Malawi. Geochemistry, Geophysics, Geosystems, 20(7), pp.3588-3607.

Wilson, T.J., 1999. Cenozoic structural segmentation of the Transantarctic Mountains rift flank in southern Victoria Land. Global and Planetary Change, 23(1-4), 105-127.

Woolley, A.R., 2001. Alkaline Rocks and Carbonatites of the World. Part 3: Africa. The Geological Society, London, p. 372.

Wright, L.J., Muirhead, J.D. and Scholz, C.A., 2020. Spatio-temporal variations in upper crustal extension across the different basement terranes of the Lake Tanganyika Rift, East Africa. Tectonics.

Zondervan, J.R., Stokes, M., Boulton, S.J., Telfer, M.W. and Mather, A.E., 2020. Rock strength and structural controls on fluvial erodibility: Implications for drainage divide mobility in a collisional mountain belt. Earth and Planetary Science Letters, 538, p.116221.

Zwaan, F., Schreurs, G., Naliboff, J., & Buiter, S. J. (2016). Insights into the effects of oblique extension on continental rift interaction from 3D analogue and numerical models. Tectonophysics, 693, 239–260.

Zwaan, F. and Schreurs, G., 2020. Rift segment interaction in orthogonal and rotational extension experiments: Implications for the large-scale development of rift systems. Journal of structural geology, 140, p.104119.

FIGURES

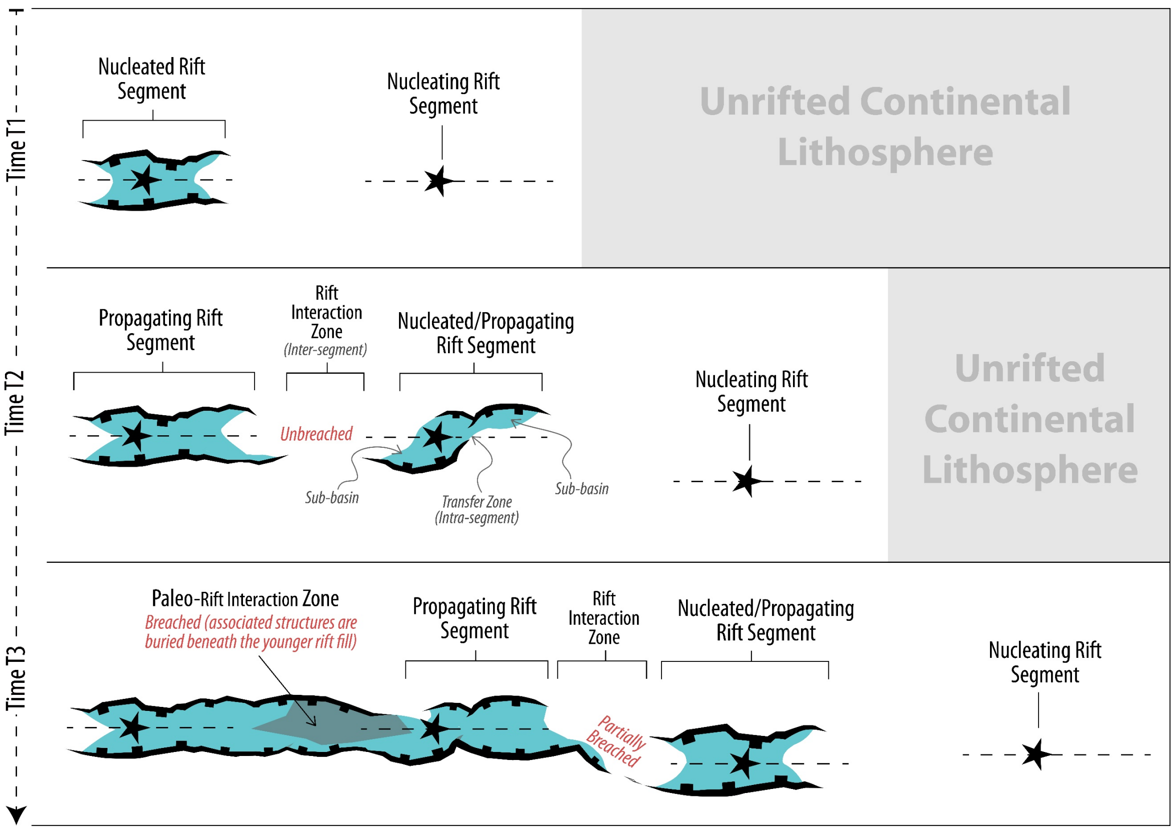

Figure 1: Simple model of nucleation and growth of rift segments along continental rift systems (modified after Nelson et al., 1992). Rift axes are represented by the black stars/dashed lines. Note that this cartoon only features collinear and underlapping parallel rift segments. For each zone of rift segment interaction, the cartoon illustrates the pre- and post-linkage geometries of the rift zones. Also, note that schematic represents rift segmentation at the early stages (stretching stage) of continental rifting; the black stars only represent hypothetical zones of rift nucleation (not spreading center as implied in Nelson et al., 1992).

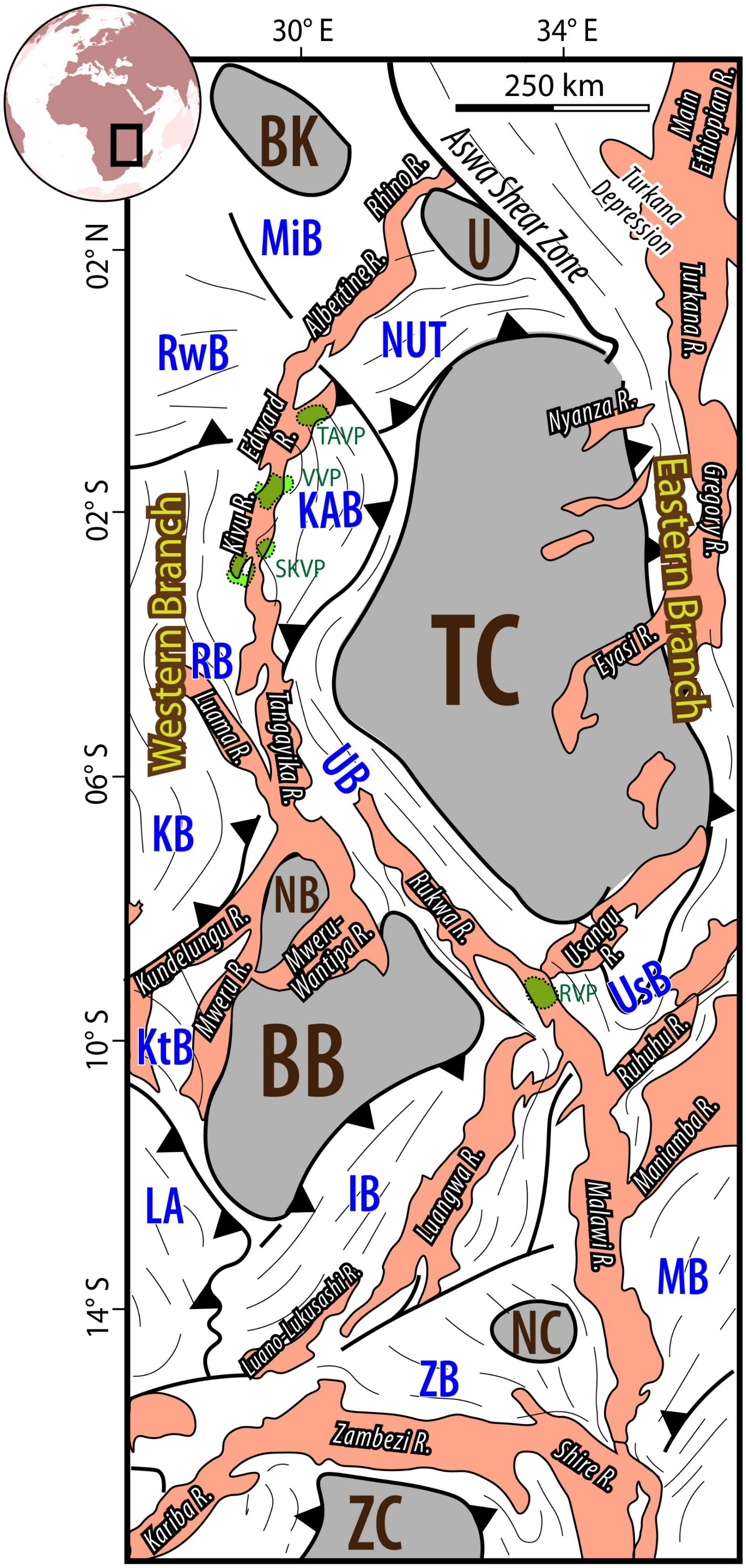

Figure 2: Map of eastern Africa showing the Precambrian basement orogenic belts with their large-scale fabric trends, cratonic blocks (grey), and rift basins (pink; includes both Mesozoic and Cenozoic rifts) modified after Daly et al. (1989). The cratons include the BB (Bangweulu Block), BK (Bomu-Kibalia Block), NC (Niassa Craton), TC (Tanzanian Craton), U (Uganda Craton), and ZC (Zimbabwe Craton). The mobile belts include IB (Irumide Belt), KAB (Karagwe-Ankole Belt), KB (Kibaran Belt), KtB (Katangan Belt), LA (Lufillian Arc), MB (Mozambique Belt), MiB (Madi-Igisi Belt), NB (North Bangweulu Microplate), NUT (North Uganda Terrane), RB (Ruzizian Belt), RwB (Ruwenzori Belt), UB (Ubendian Belt), UsB (Usagaran Belt), ZB (Zambezi Belt). Active volcanic centers along the Western Branch of the East African Rift System (green polygons) are RVP (Rungwe Volcanic Province), SKVP (South Kivu Volcanic Province), TAVP (Toro-Ankole Volcanic Province), VVP (Virunga Volcanic Province).

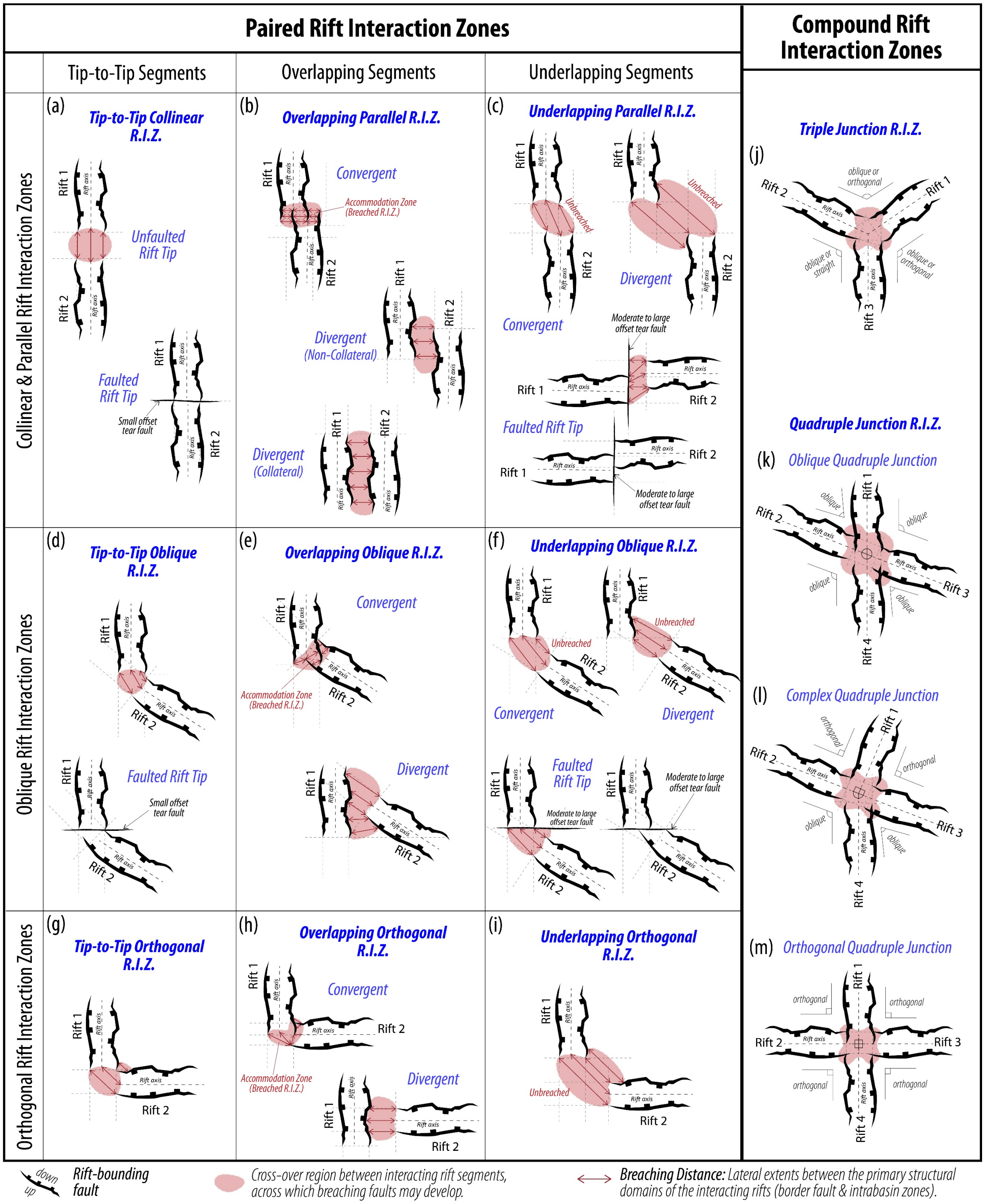

Figure 3: Classification of rift interaction zones (RIZ). The structures are not drawn to scale, but they are illustrated to represent rift segment-scale features. This broader classification is based on a review and update of the previously published classification by Nelson et al. (1992), other geometries observable in several continental rift systems (including the East African Rift System). Note that the rift segments, although presented as grabens, can also be half-grabens. The faults shown are basin-bounding fault systems.

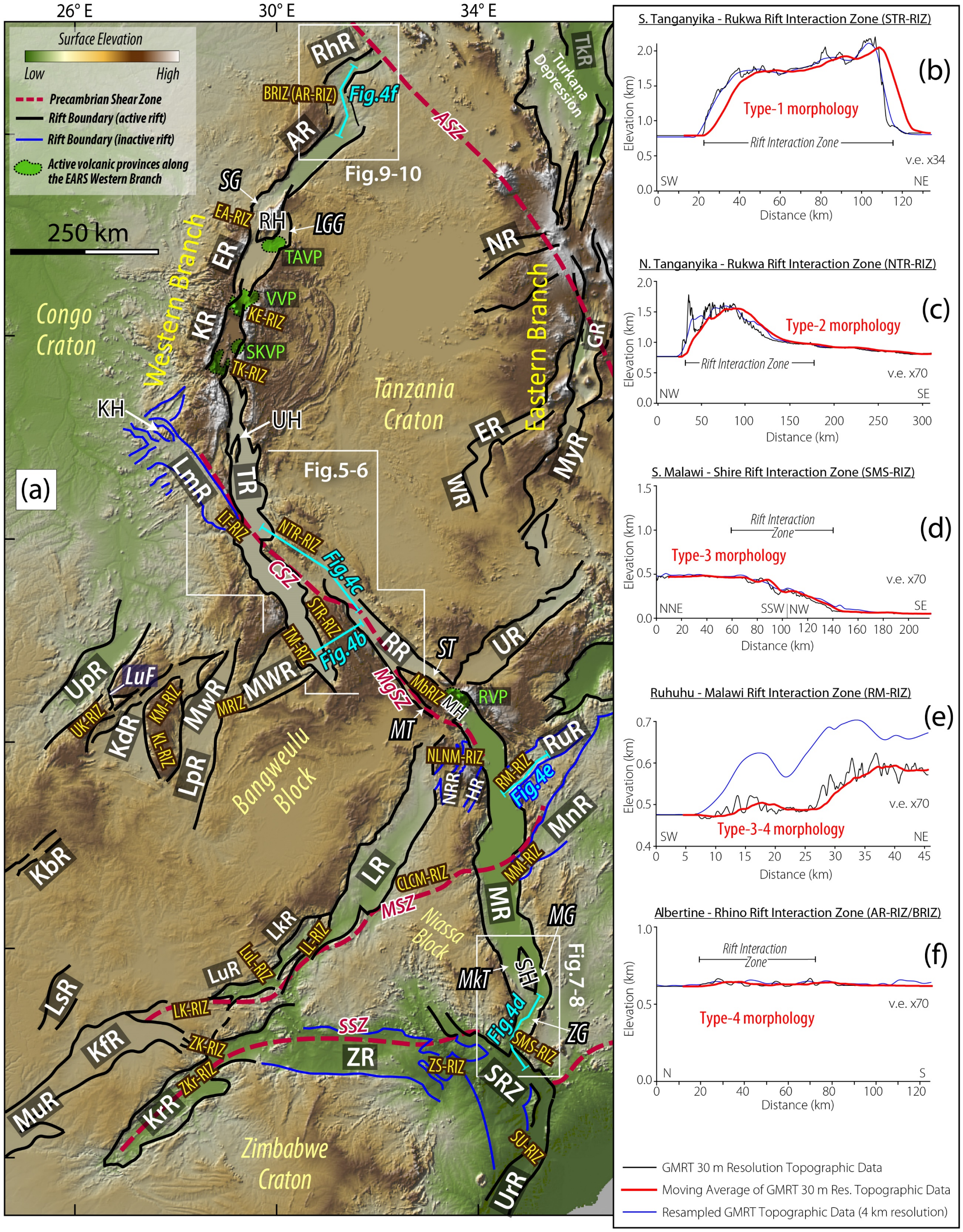

Figure 4: *Eastern Africa rift basins and the major rift interaction zones*. (a) Map of eastern Africa showing the different segments of the Cenozoic western (WB-EARS) of the East African Rift System (and some of the Eastern branch segments). Also shown are the Mesozoic rift segments that are reactivated (e.g., LR, RR, SRZ) and unreactivated (e.g., LmR, MnR, RuR, ZR) during the current phase of Cenozoic extension. AR: Albertine Rift, BRIZ (AR-

RIZ): Butiaba Rift Interaction Zone (Albertine-Rhino RIZ), CSZ: Chisi Suture Zone, CLCM-RIZ: Central Luangwa-Central Malawi Rift Interaction Zone, ER: Eyasi Rift, GR: Gregory Rift, HR: Henga Rift, KbR: Kabompo Rift, KdR: Kundelungu Rift, KfR: Kafue Rift, KH: Kabumbi Horst, KL-RIZ: Kundelungu-Luapula Rift Interaction Zone, KM-RIZ: Kundelungu-Mweru Trasfer Zone, KR: Kivu Rift, Kr: Kariba Rift, LkR: Lukusashi Rift; LGG: Lake George Graben, LK-RIZ: Luano-Kafue Rift Interaction Zone, LL-RIZ: Luangwa-Luano Rift Interaction Zone, LpR: Luapula Rift, LsR: Luansanza Rift, LT-RIZ: Luama-Tanganyika Rift Interaction Zone, LuF: Lufira Fault, LuL-RIZ: Luano-Lukusashi Rift Interaction Zone; LuR: Luano Rift, LR: Luangwa Rift, LmR: Luama Rift, MG: Malombe Graben, MgSZ: Mughesse Shear Zone, MH: Mbozi Horst, MkT: Makanjira Trough, MM-RIZ: Maniamba-Malawi Rift Interaction Zone, MnR: Maniamba Rift (a.k.a. Metangula Rift), MR: Malawi Rift, MSZ: Mwembeshi Shear Zone, MT: Musangano Trough, MRIZ: Mweru Wantipa Rift Interaction Zone, MuR: Muchili Rift, MwR: Mweru Rift, MWR: Mweru-Wantipa Rift, MyR: Manyara Rift, NLNM-RIZ: North Luangwa-North Malawi Rift Interaction Zone, NR: Nyanza Rift, NRR: North Rukuru-Mwesia Rift, NTR-RIZ: North Tanganyika-Rukwa Rift Interaction Zone, RH: Rwenzori Horst, RhR: Rhino Rift, RM-RIZ: Ruhuhu-Malawi Rift Interaction Zone, RR: Rukwa Rift, RuR: Ruhuhu Rift, RVP: Rungwe Volcanic Province, SG: Semiliki Graben, SH: Shire Horst, SKVP: South Kivu Volcanic Province, SMS-RIZ: South Malawi-Shire Rift Interaction Zone, SRZ: Shire Rift Zone, SSZ: Sanangoè Shear Zone, ST: Songwe Trough, STR-RIZ: South Tanganyika-Rukwa Rift Interaction Zone, SU-RIZ: Shire-Urema Rift Interaction Zone, TkR: Turkana Rift, TM-RIZ: Tanganyika-Mweru Wantipa Rift Interaction Zone, TR: Tanganyika Rift, TAVP: Toro-Ankole Volcanic Province, UH: Ubwari Horst, UK-RIZ: Upemba-Kundelungu Trasfer Zone (Kundelungu Horst), UpR: Upemba Rift, UR: Usangu Rift, UrR: Urema Rift, VVP: Virunga Volcanic Province, WR: Wembere Rift, ZK-RIZ: Zambezi-Kafue Rift Interaction Zone, ZKr-RIZ: Zambezi-Kariba Rift Interaction Zone, ZS-RIZ: Zambezi-Shire Rift Interaction Zone, ZR: Zambezi Rift. Map Source: Global Multi-Resolution Topography (GMRT) digital elevation model (Ryan et al., 2009). (b – f) GMRT Topographic profiles across some of the non-magmatic WB-EARS rift interaction zones, highlighting the major categories of long-wavelength cross-over relief geometries (red curves) that are observed.

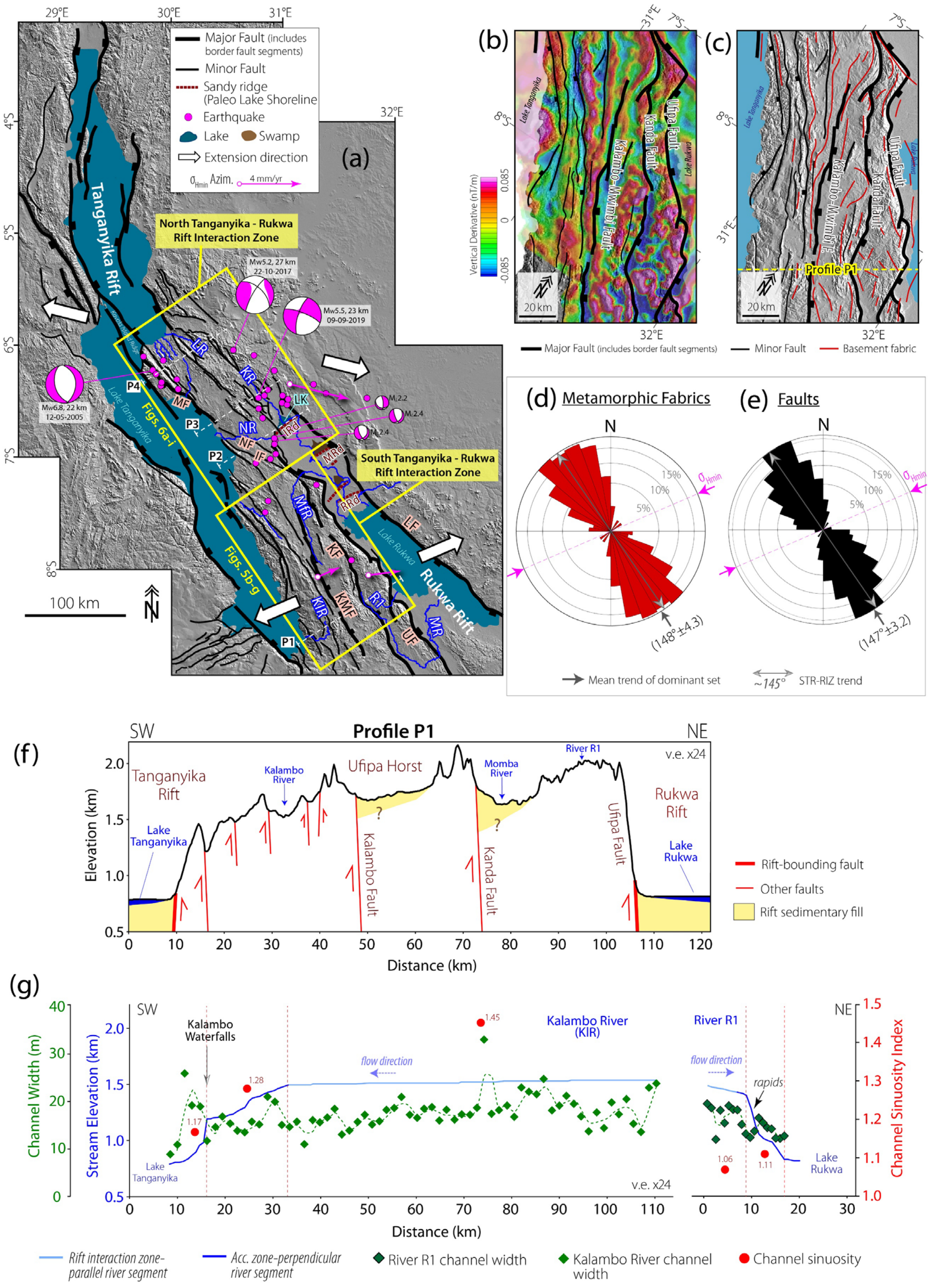

Figure 5: ***South Tanganyika–Rukwa Rift Interaction Zone, STR-RIZ (Parallel Overlapping Divergent RIZ).*** (a.) Satellite Digital Elevation Model (DEM) hillshade map of the Tanganyika Rift and the Rukwa Rift. Earthquake epicenters (Mw3.7 - 7.3) and focal mechanism solutions are from USGS and Global CMT catalogs, and Lavayssiere et al. (2019). Crustal stretching velocity (green arrows) with 95% uncertainty ellipses are from Stamps et al. (2018). IRd = Ilyandi Ridge, IF = Ifume Fault, KF = Kanda Fault System, KlR = Kalambo

River, KMF = Kalambo-Mwimbi Fault System, KR = Kavuu River, LF = Lupa Fault, LK = Lake Katavi, LR = Luegele River, MF = Mahale Fault, MfR = Mfuizi River, MR = Momba River, MRd = Maimba Ridge, NF = Nkamba Fault, NR = Nkamba River, RRd = Rungwa Ridge, UF = Ufipa Fault. Locations of the paleo-lake shore ridges are from Delvaux et al. (1998). Tanganyika Rift faults are from Muirhead et al. (2018). (b) Filtered aeromagnetic grid of the STR-RIZ, overlaid on the hillshade DEM showing the magnetic fabrics of the basement. (c) Satellite DEM hillshade map overlaid with interpretation of the interpreted basement fabrics. (d) Frequency-azimuth distribution of the aeromagnetic basement fabrics in Figure 3c. (e) Frequency-azimuth distribution of the mapped faults along the rift interaction zone (Figure 3c). (f) Rift-orthogonal topographic profile across the rift interaction zone. (g) Longitudinal stream profiles for representative axial streams in the rift interaction zone (Kalambo River and an unnamed river R1).

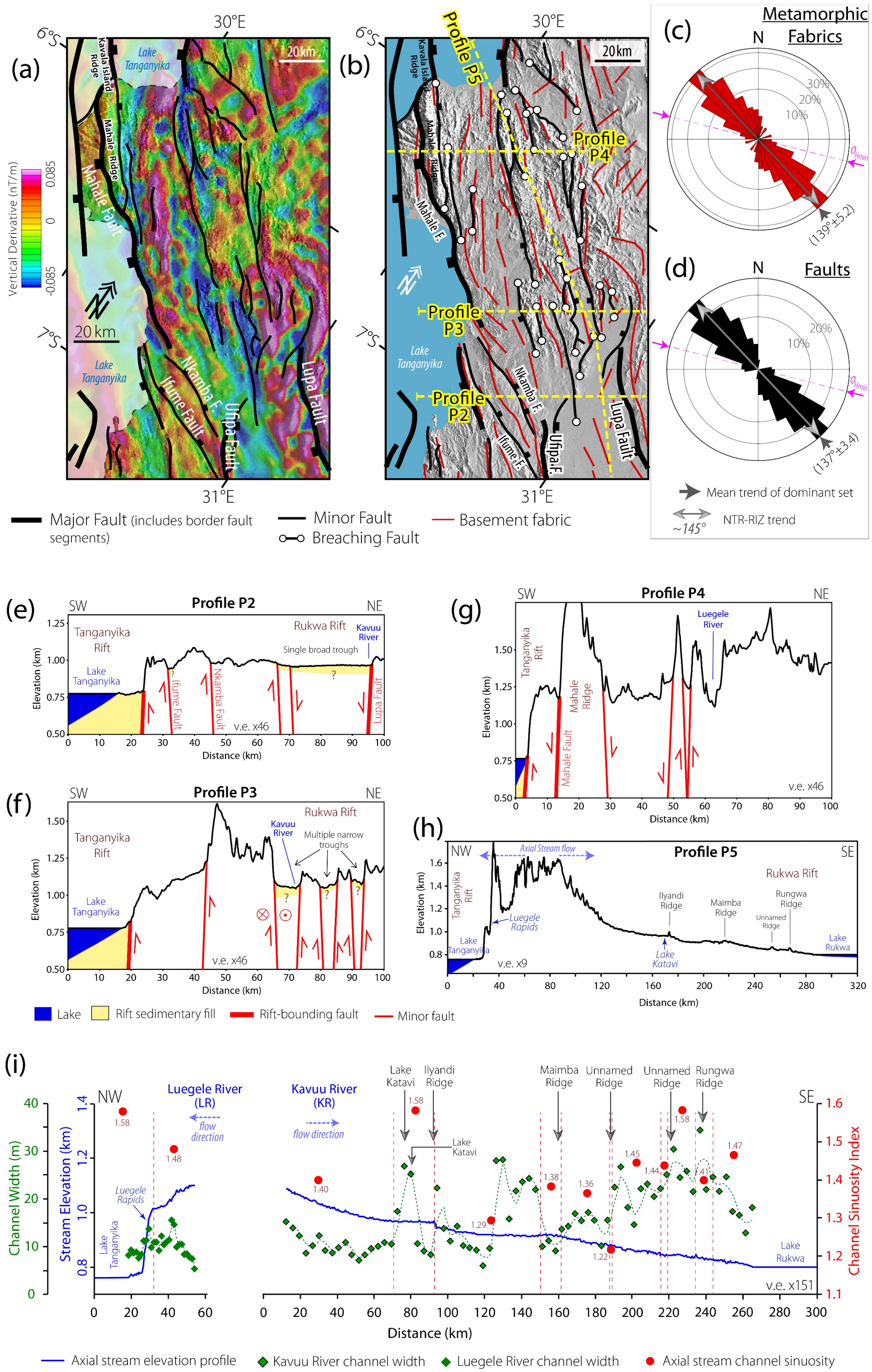
(a)
(b)
(c)
(d)
Metamorphic Fabrics
Faults
30°E
31°E
6°S
7°S
20 km
Lake Tanganyika
Kavala Island Ridge
Mahale Ridge
Mahale Fault
Nkamba F.
Ifume Fault
Ufipa Fault
Lupa Fault
Vertical Derivative (nT/m)
0.085
0
-0.085
Profile P5
Profile P4
Profile P3
Profile P2
Mahale F.
Ufipa F.
Ifume F.
N
30%
20%
10%
(139°±5.2)
(137°±3.4)
Mean trend of dominant set
NTR-RIZ trend
~145°
Major Fault (includes border fault segments)
Minor Fault
Breaching Fault
Basement fabric
(e)
Profile P2
SW
NE
Tanganyika Rift
Rukwa Rift
Kavuu River
Single broad trough
Lake Tanganyika
Ifume Fault
Nkamba Fault
Lupa Fault
v.e. x46
Elevation (km)
Distance (km)
(f)
Profile P3
Multiple narrow troughs
(g)
Profile P4
Luegele River
Mahale Ridge
Mahale Fault
(h)
Profile P5
NW
SE
Axial Stream flow
Luegele Rapids
Ilyandi Ridge
Maimba Ridge
Rungwa Ridge
Unnamed Ridge
Lake Katavi
Lake Rukwa
v.e. x9
Lake
Rift sedimentary fill
Rift-bounding fault
Minor fault
(i)
Luegele River (LR)
flow direction
Kavuu River (KR)
Lake Katavi
Ilyandi Ridge
Maimba Ridge
Unnamed Ridge
Rungwa Ridge
Channel Width (m)
Stream Elevation (km)
Channel Sinuosity Index
v.e. x151
Distance (km)
Axial stream elevation profile
Kavuu River channel width
Luegele River channel width
Axial stream channel sinuosity

Figure 6: *North Tanganyika–Rukwa Rift Interaction Zone, NTR-RIZ (Overlapping Oblique Divergent RIZ).* (a.) Filtered aeromagnetic grid of the NTR-RIZ, overlaid on satellite digital elevation model (DEM) hillshade map showing the magnetic fabrics of the basement. (b) Satellite digital elevation model (DEM) hillshade map overlaid with interpretations of the interpreted basement fabrics. (c) Frequency-azimuth distribution of the aeromagnetic basement fabrics in Figure 4b. (d) Frequency-azimuth distribution of the mapped faults along the rift interaction zone (Figure 4b). (e – g) Rift-orthogonal topographic profiles showing the southeast to northwest transition from a single broad rift geometry, through a multi-trough geometry, and attenuating into a zone of diffused faulting. (h) Interaction zone-parallel topographic profile showing the salient anomalies that characterize the morphology of the rift interaction zone. (i) Longitudinal stream profiles for the main axial streams that intersect the profile transect (Kavuu and Luegele Rivers).

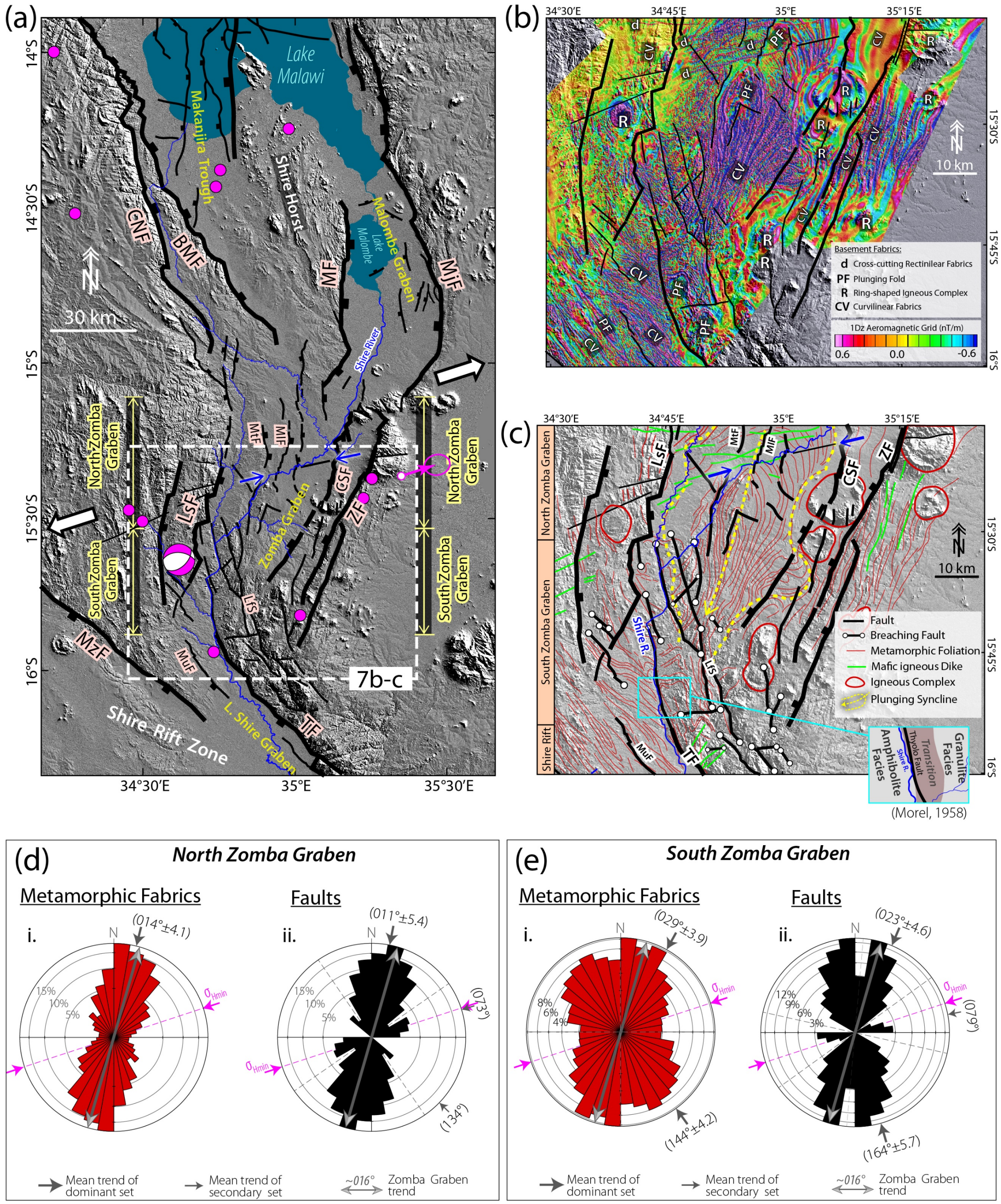

Figure 7: *South Malawi–Shire Rift Interaction Zone, SMS-RIZ (Overlapping Oblique Divergent RIZ)*. (a.) Satellite Digital Elevation Model (DEM) hillshade map with fault interpretations of the southern Malawi Rift and the northeastern part of the Shire Rift Zone. Fault lineaments are obtained from the satellite DEM and filtered aeromagnetic data interpretation (this study), and previously published satellite DEM and field study (Wedmore et al., 2020). Crustal stretching velocity (green arrow) with 95% uncertainty

ellipse is from Stamps et al. (2018). BMF = Bilila-Mtakataka Fault, CNF = Chirobwe-Ncheu Fault, LfS = Lukhubula Fault System, LsF = Lisungwe Fault, MF = Malombe Fault, Mlf = Mlungusi Fault, MtF = Mtsimukwe Fault, MuF = Mtumba Fault, MjF = Mwanjage Fault, MzF = Mwanza Fault, TF = Thyolo Fault, CSF = Chingale Step Fault, ZF = Zomba Fault. (b) Satellite DEM Hillshade map overlaid with filtered aeromagnetic grid of the rift interaction zone. (c) Interpretation of basement fabrics and faults from 7a and 7b. (d - e) Frequency-azimuth distribution of the rift faults and the inherited pre-rift basement metamorphic fabrics in the northern (North Zomba) and southern (South Zomba) domains of the rift interaction zone.

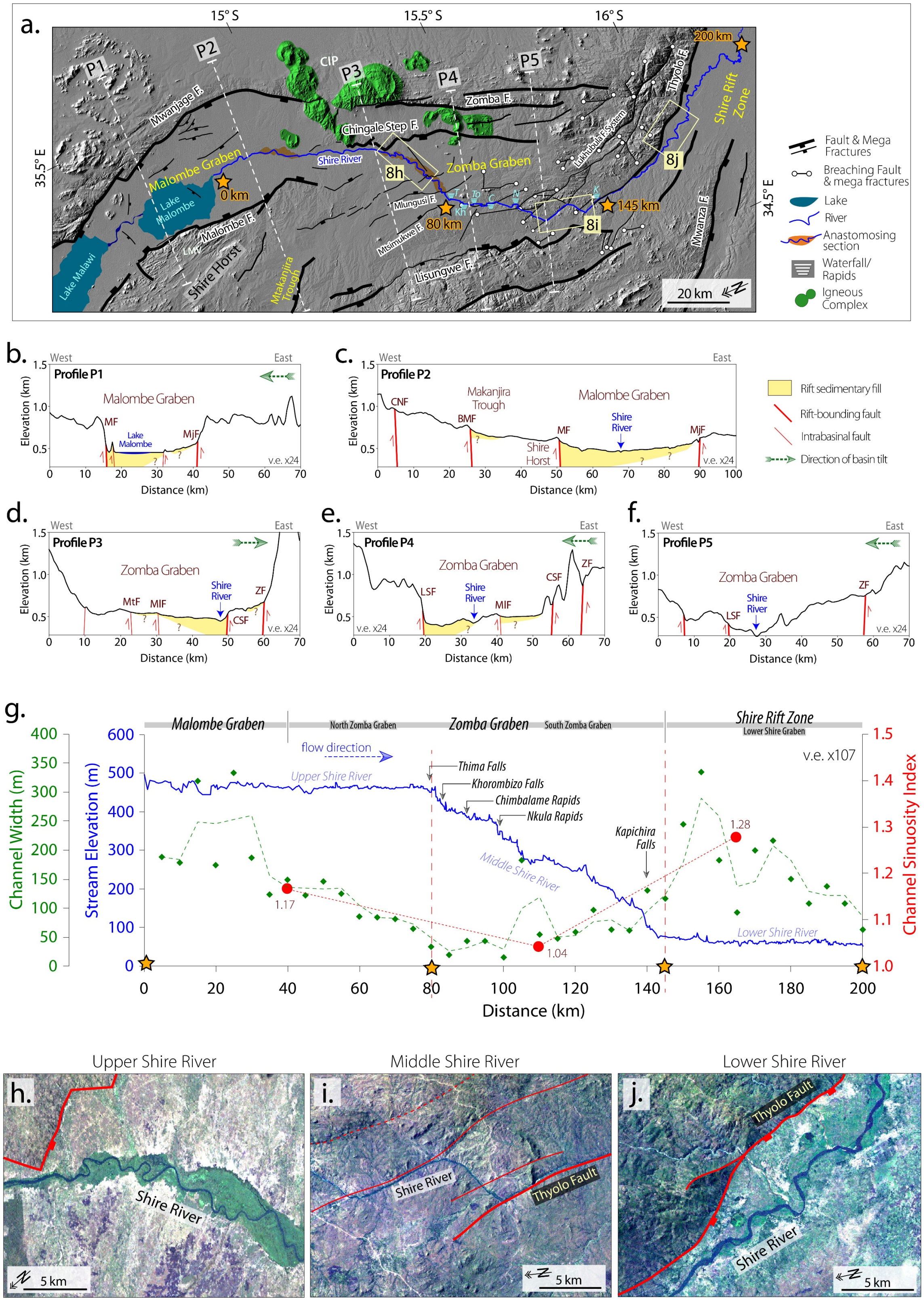
a.
15° S
15.5° S
16° S
35.5° E
34.5° E
P1
P2
P3
P4
P5
CIP
Mwanjage F.
Zomba F.
Chingale Step F.
Shire River
Malombe Graben
Zomba Graben
Lake Malombe
0 km
80 km
145 km
200 km
Malombe F.
Mlungusi F.
Msimukwe F.
Lisungwe F.
Lukhulubu F. System
Thyolo F.
Mwanza F.
Shire Rift Zone
Shire Horst
Makanjira Trough
Lake Malawi
8h
8i
8j
20 km
Fault & Mega Fractures
Breaching Fault & mega fractures
Lake
River
Anastomosing section
Waterfall/ Rapids
Igneous Complex
b.
Profile P1
Malombe Graben
MF
MjF
Lake Malombe
v.e. x24
c.
Profile P2
CNF
BMF
Makanjira Trough
Malombe Graben
MF
Shire Horst
Shire River
MjF
d.
Profile P3
Zomba Graben
MtF
MlF
Shire River
CSF
ZF
e.
Profile P4
Zomba Graben
LSF
Shire River
MlF
CSF
ZF
f.
Profile P5
Zomba Graben
Shire River
LSF
ZF
West
East
Elevation (km)
Distance (km)
Rift sedimentary fill
Rift-bounding fault
Intrabasinal fault
Direction of basin tilt
g.
Malombe Graben
North Zomba Graben
Zomba Graben
South Zomba Graben
Shire Rift Zone
Lower Shire Graben
flow direction
Upper Shire River
Thima Falls
Khorombizo Falls
Chimbalame Rapids
Nkula Rapids
Middle Shire River
Kapichira Falls
Lower Shire River
v.e. x107
1.17
1.04
1.28
Channel Width (m)
Stream Elevation (m)
Channel Sinuosity Index
Distance (km)
Upper Shire River
Middle Shire River
Lower Shire River
h.
Shire River
5 km
i.
Shire River
Thyolo Fault
5 km
j.
Thyolo Fault
Shire River
5 km

1981

Figure 8: ***Axial drainage system of the South Malawi–Shire Rift Interaction Zone, SMS-RIZ.*** (a.) Satellite digital elevation model (DEM) hillshade map overlaid with faults and the axial stream channel (Shire River). C = Chimbalame (or Machimbeya, or Chilemba) Rapids, CIP = Chilwa Igneous Province, K = Kapichira Falls, Kh = Khorombizo (or Kholombidzo) Falls, LMV = Lake Malombe Vents, N = Nkula Rapids, T = Thima Rapids, To = Toni Rapids. (b - f) Rift-orthogonal topographic profiles showing a north to south variation in rift polarity and the associated location of the Shire River. (g) Shire River stream profile, channel width, and sinuosity index estimates. (h – j) Landsat TM false color composites (321RGB) of the (h) Upper, (i) Middle, and (j) Lower courses of the Shire River. Overall, the unidirectionality of flow and morphology of the axial stream across the rift interaction zone cross-over region, linkage of interacting rift border faults by a cluster of breaching fault/fractures, exposure of pre-rift basement at the rift-floor (Figure 8i), and an unequilibrated stream profile (Figure 8g) suggest a recent breaching of the rift interaction zone.

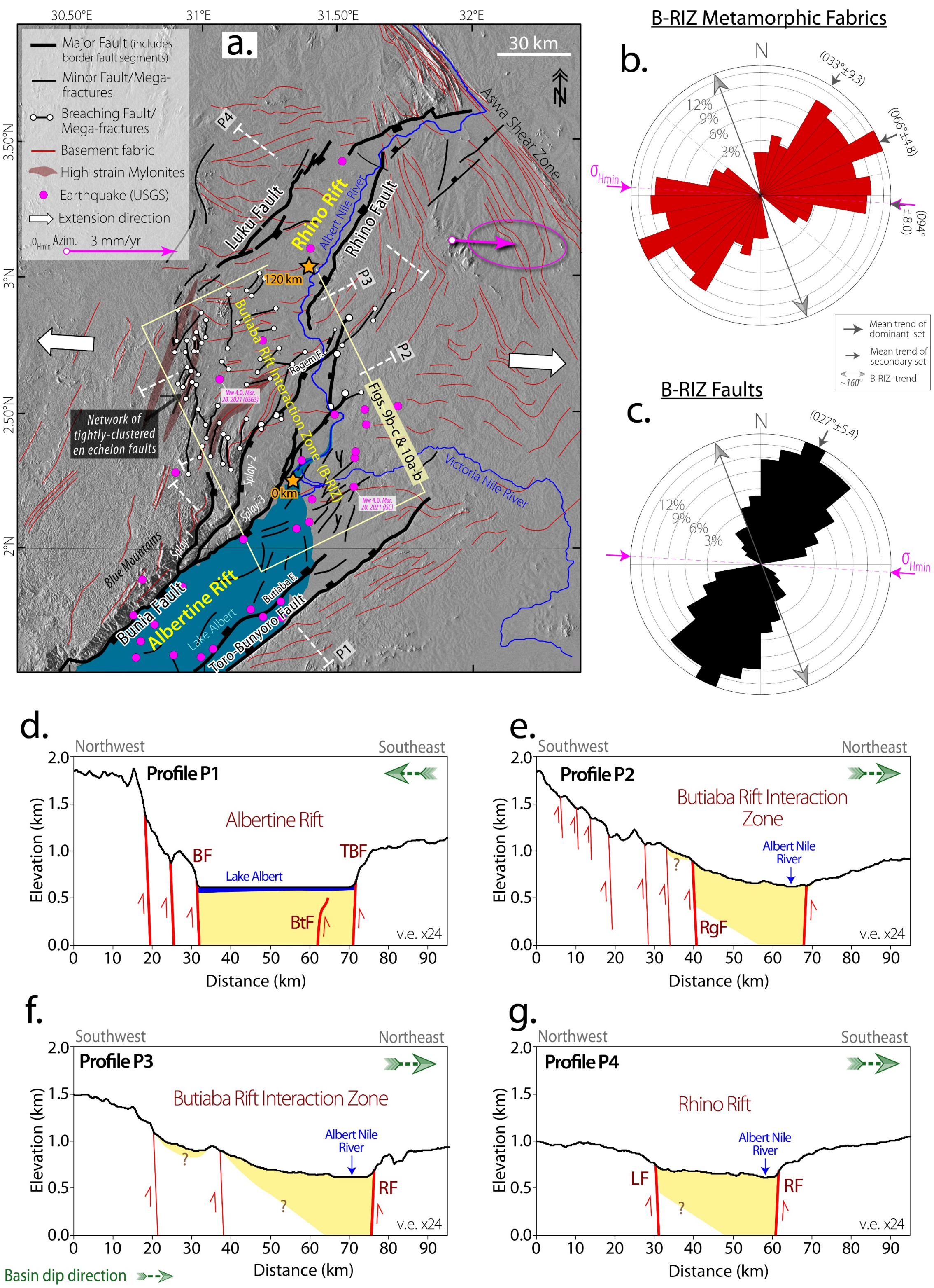

a.
30.50°E
31°E
31.50°E
32°E
3.50°N
3°N
2.50°N
2°N
30 km
N
Major Fault (includes border fault segments)
Minor Fault/Mega-fractures
Breaching Fault/ Mega-fractures
Basement fabric
High-strain Mylonites
Earthquake (USGS)
Extension direction
Azim. 3 mm/yr
Aswa Shear Zone
Rhino Rift
Rhino Fault
Luku Fault
Albert Nile River
Butiaba Rift Interaction Zone (B-RIZ)
Figs. 9b-c & 10a-b
Network of tightly-clustered en echelon faults
Victoria Nile River
Blue Mountains
Bunia Fault
Albertine Rift
Lake Albert
Toro-Bunyoro Fault
Butiaba F.
Ragem F.
Splay-2
Splay-3
120 km
0 km
P1
P2
P3
P4
B-RIZ Metamorphic Fabrics
b.
N
(033°±9.3)
(066°±4.8)
(094°±8.0)
12%
9%
6%
3%
σHmin
Mean trend of dominant set
Mean trend of secondary set
~160° B-RIZ trend
B-RIZ Faults
c.
N
(027°±5.4)
12%
9%
6%
3%
σHmin
d.
Northwest
Southeast
Profile P1
Albertine Rift
BF
TBF
Lake Albert
BtF
v.e. x24
Elevation (km)
Distance (km)
e.
Southwest
Northeast
Profile P2
Butiaba Rift Interaction Zone
Albert Nile River
RgF
v.e. x24
Elevation (km)
Distance (km)
f.
Southwest
Northeast
Profile P3
Butiaba Rift Interaction Zone
Albert Nile River
RF
v.e. x24
Elevation (km)
Distance (km)
g.
Northwest
Southeast
Profile P4
Rhino Rift
Albert Nile River
LF
RF
v.e. x24
Elevation (km)
Distance (km)
Basin dip direction

Figure 9: ***Albertine–Rhino Rift Interaction Zone, AR-RIZ, a.k.a. Butiaba Rift Interaction Zone, BRIZ (Underlapping Parallel Divergent RIZ).*** (a.) Satellite digital elevation model (DEM) hillshade map overlaid with interpretations of fault and basement fabrics in the Albertine and Rhino Rifts. Fault lineaments are interpreted from satellite DEM and filtered aeromagnetic data (this study; Supplementary Figure 3), and from seismic reflection data (Simon et al., 2017). We also interrogated and included faults segments from other previous studies (GTK Consortium, 2012; Westerhof et al., 2014; Katumwehe et al., 2015). The locations of highly strained mylonites are obtained from Westerhof et al. (2014). Crustal stretching velocity (green arrow) with 95% uncertainty ellipse is from Saria et al. (2014). (b – c) Frequency-azimuth distribution of the basement fabrics (b) and faults (c) in the rift interaction zone. (d - g) Rift-orthogonal topographic profiles showing a southwest to northeast variation in rift polarity in relation to the location of the axial stream. BF = Bunia Fault, BtF = Butiaba Fault, LF = Luku Fault; RF = Rhino Fault, RgF = Ragem Fault, TBF = Toro-Bunyoro Fault. Note that the thickness of the rift sedimentary deposits shown in the topographic profiles are not drawn to scale.

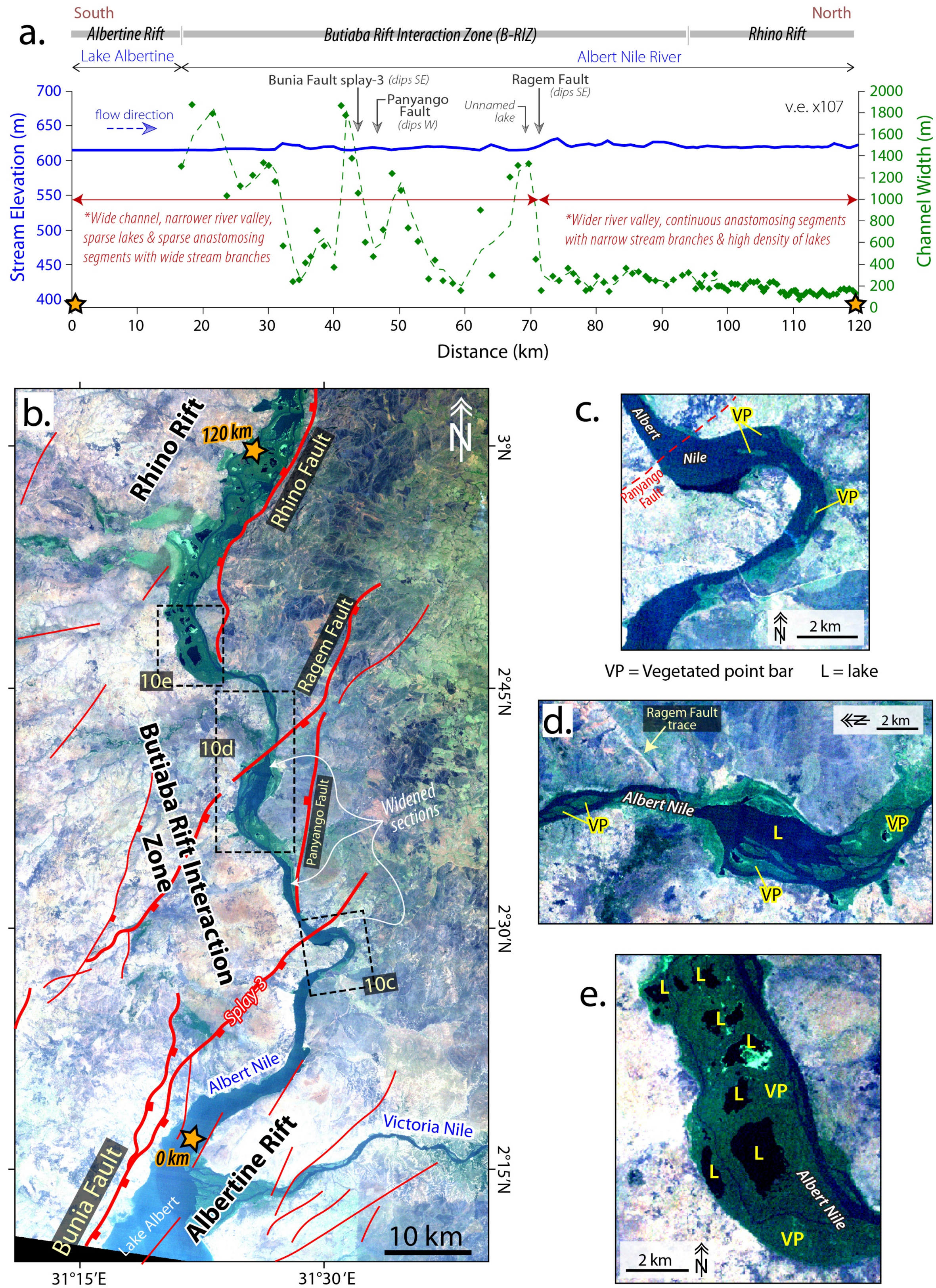
a.
South
North
Albertine Rift
Butiaba Rift Interaction Zone (B-RIZ)
Rhino Rift
Lake Albertine
Albert Nile River
Bunia Fault splay-3 (dips SE)
Panyango Fault (dips W)
Unnamed lake
Ragem Fault (dips SE)
v.e. x107
flow direction
*Wide channel, narrower river valley, sparse lakes & sparse anastomosing segments with wide stream branches
*Wider river valley, continuous anastomosing segments with narrow stream branches & high density of lakes
Stream Elevation (m)
Channel Width (m)
Distance (km)
b.
Rhino Rift
120 km
Rhino Fault
Ragem Fault
10e
10d
10c
Butiaba Rift Interaction Zone
Panyango Fault
Widened sections
Splay-3
Albert Nile
Victoria Nile
0 km
Albertine Rift
Bunia Fault
Lake Albert
10 km
3°N
2°45'N
2°30'N
2°15'N
31°15'E
31°30'E
c.
Albert
Nile
Panyango Fault
VP
2 km
VP = Vegetated point bar
L = lake
d.
Ragem Fault trace
Albert Nile
VP
L
2 km
e.
L
VP
Albert Nile
2 km

Figure 10: ***Axial drainage system of the Albertine–Rhino Rift Interaction Zone (Butiaba Rift Interaction Zone).*** (a.) The Albert Nile River stream profile, and along-channel stream width. At the anastomosing segments of the river, the profile represents a single branch of the river with open waters (i.e., not covered by wetland vegetation). (b - e) Landsat TM false color composite (321RGB) images showing the sinuous and anastomosing morphology of the Albert Nile River within the rift interaction zone. L = Lake, VP = vegetated point bar.

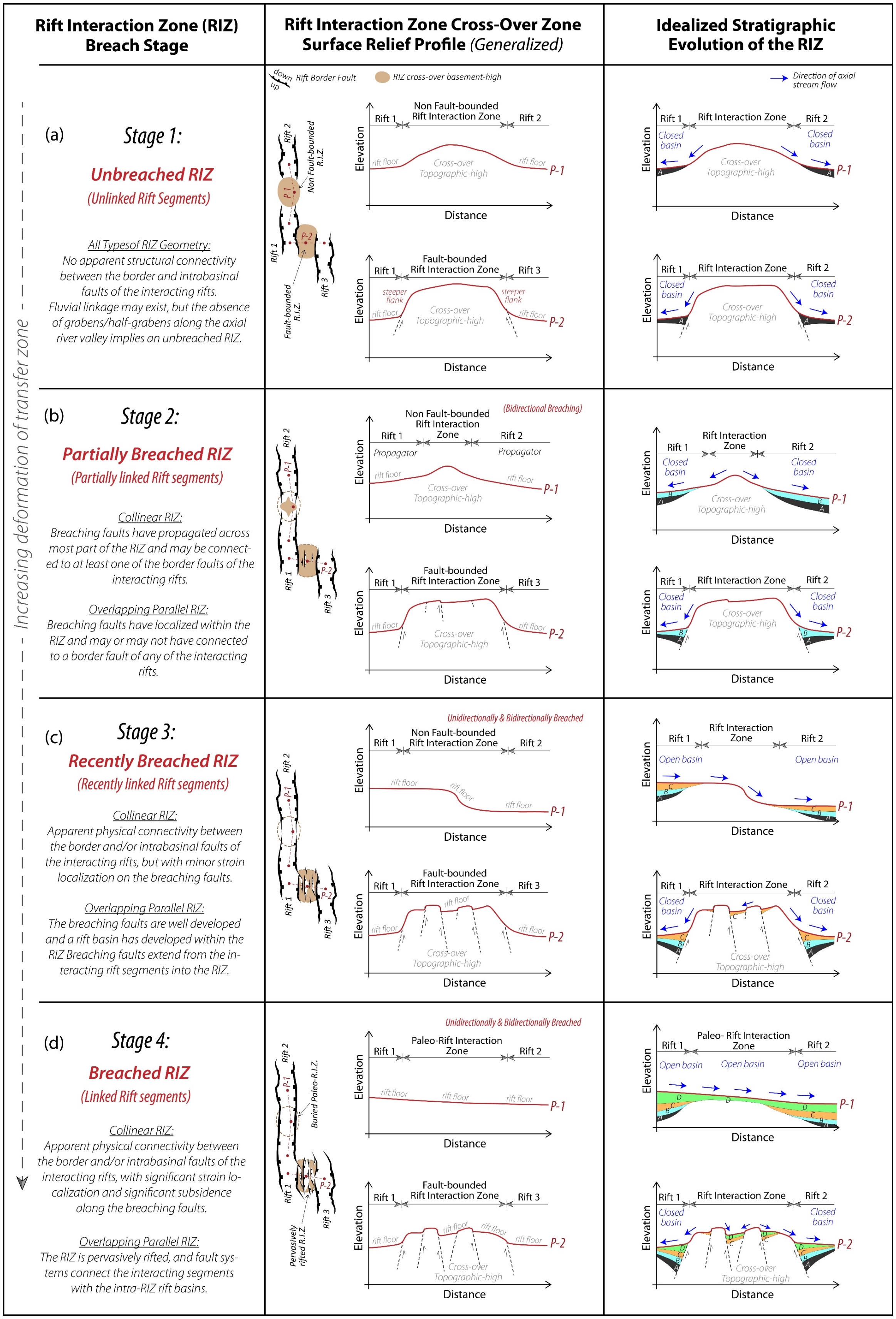
Rift Interaction Zone (RIZ) Breach Stage
Rift Interaction Zone Cross-Over Zone Surface Relief Profile (Generalized)
Idealized Stratigraphic Evolution of the RIZ
Rift Border Fault
RIZ cross-over basement-high
Direction of axial stream flow
Increasing deformation of transfer zone
(a) Stage 1:
Unbreached RIZ
(Unlinked Rift Segments)
All Typesof RIZ Geometry:
No apparent structural connectivity between the border and intrabasinal faults of the interacting rifts.
Fluvial linkage may exist, but the absence of grabens/half-grabens along the axial river valley implies an unbreached RIZ.
(b) Stage 2:
Partially Breached RIZ
(Partially linked Rift segments)
Collinear RIZ:
Breaching faults have propagated across most part of the RIZ and may be connected to at least one of the border faults of the interacting rifts.
Overlapping Parallel RIZ:
Breaching faults have localized within the RIZ and may or may not have connected to a border fault of any of the interacting rifts.
(c) Stage 3:
Recently Breached RIZ
(Recently linked Rift segments)
Collinear RIZ:
Apparent physical connectivity between the border and/or intrabasinal faults of the interacting rifts, but with minor strain localization on the breaching faults.
Overlapping Parallel RIZ:
The breaching faults are well developed and a rift basin has developed within the RIZ Breaching faults extend from the interacting rift segments into the RIZ.
(d) Stage 4:
Breached RIZ
(Linked Rift segments)
Collinear RIZ:
Apparent physical connectivity between the border and/or intrabasinal faults of the interacting rifts, with significant strain localization and significant subsidence along the breaching faults.
Overlapping Parallel RIZ:
The RIZ is pervasively rifted, and fault systems connect the interacting segments with the intra-RIZ rift basins.
Non Fault-bounded Rift Interaction Zone
Fault-bounded Rift Interaction Zone
Paleo-Rift Interaction Zone
(Bidirectional Breaching)
Unidirectionally & Bidirectionally Breached
Rift 1
Rift 2
Rift 3
Elevation
Distance
Cross-over Topographic-high
rift floor
steeper flank
Propagator
Closed basin
Open basin
P-1
P-2
Non Fault-bounded R.I.Z.
Fault-bounded R.I.Z.
Buried Paleo-R.I.Z.
Pervasively rifted R.I.Z.

Figure 11: ***Models of the stages of evolution of non-magmatic rift interaction zones**.* (a – d) Summary cartoons based on the general observations of breaching fault patterns, long-wavelength topographic relief, and axial drainage patterns of rift interaction zones along the western branch of the East African Rift System (WB-EARS). We present only the tip-to-tip parallel and overlapping parallel divergent rift interaction zone geometries as examples, to illustrate our observations and idealized models. The models assume: 1) a humid continental setting, 2) orthogonal extension, 3) the erodibility of the pre-rift basement is relatively uniform (in the case of the WB-EARS rift interaction zones studied), 4) sediment supply in the interacting basins keeps up with strain rates on faults, and 5) no active dynamic topography in the deforming rift interaction zone. The geometry of the breaching faults as presented, are simplified and do necessarily indicate the kinematics of the breaching structures. Also, note that the topographic relief shapes of Stages 2 (and possibly Stage 3) are implied to strongly depend on the directionality of propagation of rift linkage assuming that basement erodibility is uniform. Although our models are based on regions of active early-stage (stretching phase) continental rifting in which at least one of the interacting rift pairs is active, the observations are relevant for buried rift interaction zones in ancient rift settings.

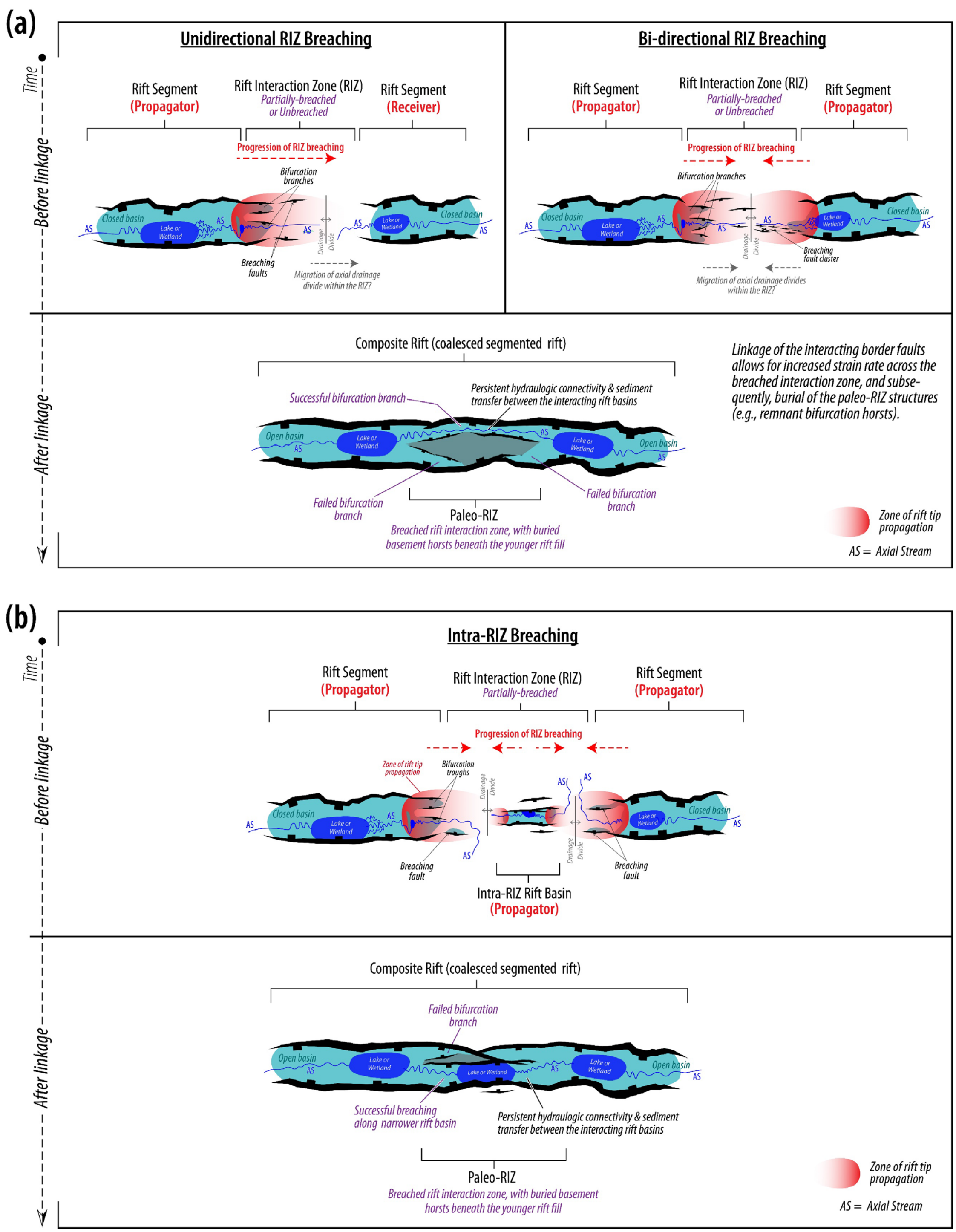

Figure 12: ***Directional propagation of rift interaction zone breaching, and rift-tip interactions.*** Using an active collinear rift interaction zone as a simple example, these cartoons show directionality of rift interaction zone breaching and rift tip splay as an example of rift-tip interactions. Other rift tip interactions discussed in the study include border fault rotation and fault cluster networks.

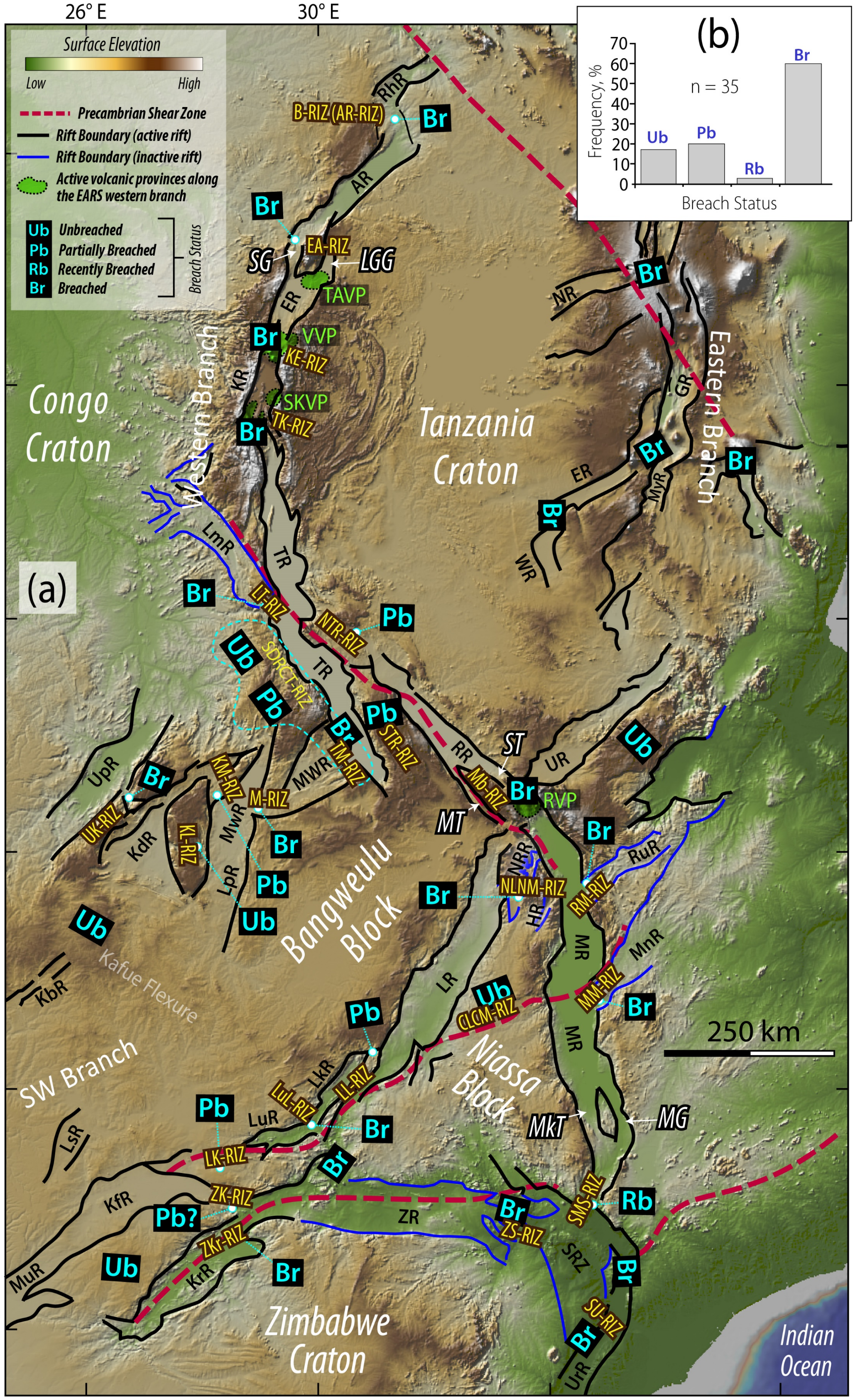
26° E
30° E
02° N
02° S
06° S
10° S
14° S
18° S
Surface Elevation
Low
High
Precambrian Shear Zone
Rift Boundary (active rift)
Rift Boundary (inactive rift)
Active volcanic provinces along the EARS western branch
Ub Unbreached
Pb Partially Breached
Rb Recently Breached
Br Breached
Breach Status
(a)
(b)
Frequency, %
n = 35
Breach Status
Ub
Pb
Rb
Br
Congo Craton
Tanzania Craton
Bangweulu Block
Niassa Block
Zimbabwe Craton
Western Branch
Eastern Branch
SW Branch
Kafue Flexure
Indian Ocean
250 km
B-RIZ (AR-RIZ)
RhR
AR
EA-RIZ
SG
LGG
TAVP
ER
VVP
KE-RIZ
KR
SKVP
TK-RIZ
LmR
TR
LT-RIZ
NTR-RIZ
SDRCT-RIZ
STR-RIZ
TM-RIZ
RR
ST
UR
Mb-RIZ
RVP
MT
UpR
UK-RIZ
KdR
KM-RIZ
M-RIZ
MwR
MWR
KL-RIZ
LpR
NRR
NLNM-RIZ
RM-RIZ
RuR
HR
MR
MnR
MM-RIZ
LR
CLCM-RIZ
KbR
LkR
LL-RIZ
LuL-RIZ
LuR
LsR
LK-RIZ
KfR
ZK-RIZ
Pb?
ZR
ZS-RIZ
SRZ
SMS-RIZ
ZKr-RIZ
KrR
MuR
MkT
MG
SU-RIZ
UrR
NR
GR
MyR
WR

Figure 13: ***Breach-state of rift interaction zones in eastern Africa.*** (a) Map showing the inferred breach state of the rift interaction zones along the western, SW, and SE branches of the East African Rift System, inferred from the general conventions of rift interaction zone cross-over structure and physiography proposed in this study. Also note that we characterize all magmatic rift interaction zones as "breached" because of the lithospheric-scale deformation associated with magmatism. SDRCT-RIZ = South DRC Rift Zone - Tanganyika Rift Interaction Zone. See Figure 4a for the explanations of the abbreviated rift and interaction zone labels. Map Source: Global Multi-Resolution Topography (GMRT) digital elevation model (Ryan et al., 2009). (b) Histogram of the distribution of the inferred breach states of the rift interaction zones in Figure 13a.